STRUCTURAL AND DOWNSHIFTING PROPERTIES OF $CaMoO_4$:Eu THROUGH Gd^{3+} CO-DOPING

In this chapter structural and photo-physical study on Eu^{3+} activated $CaMoO_4$ via Gd^{3+} co-doping has been reported. The Eu^{3+}/Gd^{3+} doped $CaMoO_4$ system fluoresce in red color when excited with 266 nm radiation. In the present studies 266 nm excitation is used to get the downconversion emissions. The studies have been divided into two parts:

Part 1: Influence of Gd^{3+} co-doping on structural properties of $CaMoO_4$:Eu nano-particles

Part 2: Enhanced Photoluminescence in $CaMoO_4$:Eu^{3+} by Gd^{3+} co-doping

Part 1

4.1 Influence of Gd^{3+} co-doping on structural properties of $CaMoO_4$:Eu nanoparticles

4.1.1 Introduction

Recently, alkaline-earth metal tungstates and molybdates (scheelite type, ABO_4, A = Ca^{2+}, Sr^{2+}, Mg^{2+} and Ba^{2+}; B = Mo and W) based derivatives are important host material for rare-earth-doped phosphors because of their excellent optical and physical properties such as excellent strength, chemical, thermal stabilities, high decomposition temperature and multi-color range from blue to green-yellow-red [Raju, et al.(2012), Parchur, et al.(2011a), Cavalli, et al.(2010), Mahlik et al.(2013), Parchur et al.(2012a)]. Among the alkaline-earth metal molybdates, $CaMoO_4$ (having space group $I4_{1/a}$ having point group symmetry C^6_{4h} with tetragonal structure) has been used in solid-state laser, scintillators in medical devices, solar cell and fiber-optical communication [Raju, et al.(2012), Parchur, et al.(2011b), Cavalli, et al.(2010), Mahlik, et al.(2013), Parchur, et al.(2012a), Marques et al.(2010), Cavalcante, et al.(2012), Longo, et al.(2011)]. In $CaMoO_4$, Mo^{6+} is coordinated by four oxygen atoms in tetrahedral symmetry to form MoO_4 and Ca has been coordinated by 8 oxygen atoms to form CaO_8 [Marques, et al.(2010), Longo, et al.(2011), Parchur, et al.(2011a)]. [MoO_4^{2-}] tetrahedron unit efficiently absorbs light with higher absorption cross section near UV region and its photoluminescence shows broad visible range. The

photoluminescence of $CaMoO_4$ doped with different lanthanide ions has been studied in order to get different colours [Parchur, et al.(2012a)]

Recently, nanomaterials have been synthesized in the form of nanorods, sheets, wires, nanopores and core-shell [Acharya, et al.(2008), Ariga, et al.(2012), Vinu and ariga (2013), Kar and Patra (2012)]. Lanthanide (Ln^{3+}) doped inorganic nanomaterials are used in luminescence applications because of resistant to photo-bleaching, superior photochemical stability, sharp emission bands, persistent photoluminescence lifetime, high chemical stability and low toxicity [Gupta, et al.(2011)]. Moreover, Ln^{3+} ion such as Gd^{3+} has large number of unpaired electrons in 4f orbital's which can change the relaxation time of surrounding water protons when Ln^{3+} doped nanomaterials are dispersed in water. Thus, these are also used as MRI (magnetic resonance imaging) contrast agent in medical diagnostics [Guo, et al.(2010), Nunez, et al. (2013)]. There are reports on enhancement of luminescence by core-shell, co-doping and energy transfer process [Podhorodecki, et al.(2010a), Podhorodecki, et al.(2009a), Podhorodecki, et al.(2010b), Podhorodecki, (2009b)]. Therefore, systematic research on the synthesis protocol, structure and its resultant effects on phosphor characteristics is necessary and worthy of pursuit. Moreover influence of Gd^{3+} incorporation on structural and luminescence properties of $CaMoO_4$:Eu has not been explored in literature in much detail. Many synthesis processes have been reported by different groups to synthesize $CaMoO_4$ with or without Ln^{3+} ions via Czochralski, conventional solid state reaction method, sol-gel, hydrothermal, co-precipitation and polyol methods [Parchur, et al. (2012a), Yu, et al. (2007)]. Auto-combustion methods has been proven to be very much effective as one have wide range of flexibility of selecting fuels, rapid cooling process which hinders the nucleation growth of the crystallites, enabling non-agglomerated nanocrystals of high purity with nano-size regime. This methodology makes it possible to prepare nonmaterial with versatile compositions of different concentrations which is easily doped with various ions [Qiu, et al.(2007)].

In this chapter, we have prepared Gd^{3+} (0, 2, 5, 7 and 10 at.%) co-doped $CaMoO_4$:Eu nanoparticles via efficient combustion technique. Here, the urea-nitrate combustion synthesis is used. For the optimal Eu^{3+} concentration (2 at.% in our case), effect of Gd^{3+} co-doping on structure, chemical binding energies and morphology of $CaMoO_4$:Eu has been investigated in detail for as-prepared, 600 and 900 ^oC annealed samples.

4.1.2 Experimental

4.1.2.1 Sample Preparation

Combustion synthesis route was employed in order to synthesize the nanophosphors at lower temperature with high chemical homogeneity. $CaCO_3$ (99.99%, Sigma Aldrich), Eu_2O_3 (99.99%, Alfa Aesar) and Gd_2O_3 (99.99%, Alfa Aesar) and $(NH_4)_6Mo_7O_{24}.4H_2O$ (99%, Alfa Aesar) were used as a starting materials. In a typical synthesis process (e. g. 2 at.% Gd^{3+}, 2 at.% Eu^{3+} doped $CaMoO_4$), 0.343 g of $CaCO_3$, 0.631 g of $(NH_4)_6Mo_7O_{24}.4H_2O$, 0.126 g of Eu_2O_3 and 0.129 g of Gd_2O_3 were dissolved together in 2 ml of 1 M nitric acid (HNO_3). The mixture was heated at 80 ^oC for the removal of excess of acid and this process was repeated at least five times with addition of 5 ml doubled distilled water. Transparent solution is obtained after 1 hour. $(NH_4)_6Mo_7O_{24}.4H_2O$ was dissolved in 20 ml of deionised water. To this 2 g of urea was added for adjusting the pH of the solution between 8 and 9 and placed under sonication for 30 min. This was added to above solution drop wise and stirred for 2-3 h. A whitish gel like precipitate was obtained. This was placed in furnace at ~250 ^oC for 30 min to take place auto combustion. Powder sample so obtained was treated as as-prepared sample (ASP). ASP samples are divided into three parts. One part of the sample was annealed at 600 ^oC while other part at 900 ^oC for 4 h in ambient atmosphere at the rate of 2 ^oC min^{-1} in programmable electrical furnace and remaining third part was kept as such.

4.1.2.2 Characterization techniques

Structural confirmation of the phosphor was identified by X-ray diffraction (XRD) using a Rigaku miniflex-II diffractometer equipped with Ni filter using CuK_α radiation (1.5405 Å) at ~30 kV and ~15 mA in the range $10 \leq 2\theta/^o \leq 70^o$ with a step size of $\Delta 2\theta = 0.02^o$. The Fourier transform infrared (FTIR) spectrum of the sample was recorded on a Perkin - Elmer 580 B IR spectrometer using the KBr pellet technique in the range 4000-400 cm^{-1}. Sample was mixed with KBr (Sigma Aldrich, 99.99%) in 1:5 wt.% ratio and transparent pellet was prepared. The chemical bonding energies of the respective ions in the sample were measured using X- ray photoelectron spectroscopy (XPS) SPECS, Germany (Mg K_α X-ray source, $h\nu$ = 1253.6 eV). Differential thermal (DT) and thermo-gravimetric (TG) analyses of the sample were carried out with a Material Analysis and Characterization TG-DTA 2000 with a heating rate of 5 ^oC/min. Morphology of synthesized powder samples was further examined by a field emission scanning electron

microscope (FESEM, JSM-6700, model JEOL, Japan). Coating of osmium had been sprayed on the sample surfaces using a Hitachi (Japan) fine coat ion sputter E-1010 unit to avoid the expected charging of the specimens before FESEM observation was performed on each time. Field emission transmission electron microscope (FE-TEM) equipped with energy disperse X-ray spectroscopy, EDX (FETEM, JEM-2100F, JEOL, Japan) operating at an accelerating voltage of 200 kV were employed for the inspection of morphology of the samples. EDX analysis was used to confirm the presence of the constituent elements in the sample. For the TEM measurement a small amount of Gd^{3+} co-doped $CaMoO_4$:Eu was dispersed in the methanol and placed under sonication for 30 min. A few drops of suspended monodispersed colloidal solution were put over a carbon coated copper grids. Measurements were performed on these grids after drying the samples naturally.

4.1.3 Results and Discussion

4.1.3.1 Structural Analysis

4.1.3.1.1 XRD study

XRD patterns of ASP Gd^{3+} (0, 2, 5 7 and 10 at.%) co-doped sample of $CaMoO_4$:Eu is shown in the Figure 4.1(a). It is evident from the figure that even as-prepared (ASP) sample shows highly crystalline behaviour with tetragonal structure. All diffraction peaks match well with JCPDS card no. 29:0351 (a = 5.226 Å, c = 11.43Å and V = 312.17Å^3). In the case of Gd^{3+}(2, 5, 7 and 10 at.%) co-doped ASP samples, some extra XRD peaks (marked with #) are observed at an angle 2θ = ~17, 19.47, 25.98, 27.39, 35.48 and 42.7°. Such peaks are not matching with JCPDS card no. 29-0351. The intensity of these extra peak intensities increase as doping concentration of Gd^{3+} increases. Also some extra peaks are found at ~23.3, 25.6 and 26.9° for 10 at.% Gd^{3+} co-doped samples of $CaMoO_4$:Eu annealed at 600 °C. These extra peaks may be due to the $MoO_n.mH_2O$ (where m and n are numbers), carbonate, water complexes, Gd-Eu-O related compounds, or Eu^{3+} oxides present in the sample. These phases are not identified in this study. Similar types of observations have been reported for Tb^{3+} doped $CaMoO_4$ [Parchur, et al.(2012a)]. However, in case of 900 °C annealed samples, no other traces of impurity phases have been observed. However, the intensities of diffraction peaks slightly decrease at higher Gd^{3+} co-doping concentrations.

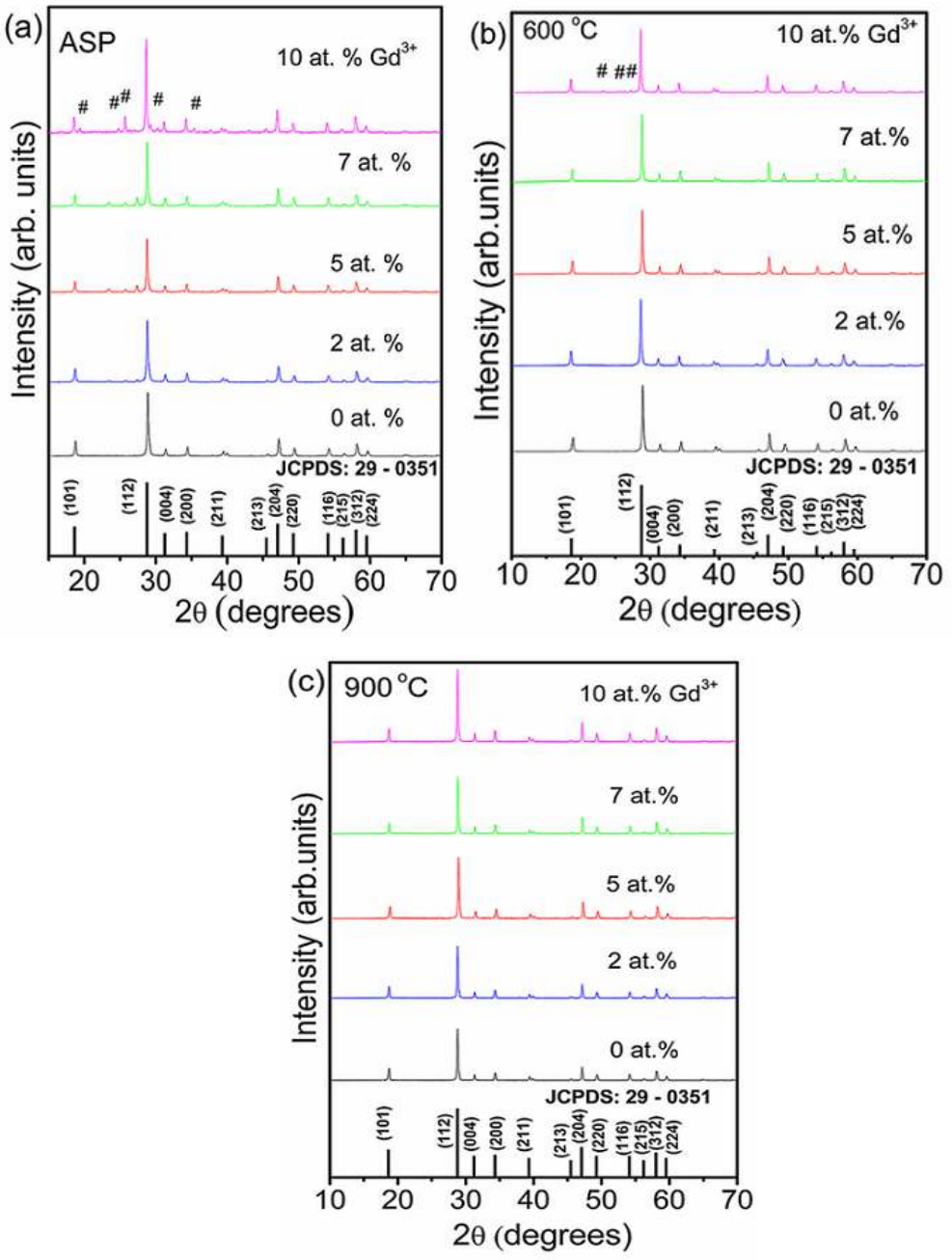

Figure 4.1: (a), (b) and (c) XRD patterns of Gd^{3+}(0, 2, 5, 7 and 10 at.%) co-doped $CaMoO_4$:Eu for ASP, 600 and 900 °C samples, respectively. Atomic percentage of Gd^{3+} is given in figure itself. The symbol # represents the extra phase evolution.

Lattice parameters of typical 5 at.% Gd^{3+}co-doped $CaMoO_4$:Eu for ASP are a = 5.239Å, c = 11.392Å, V = 313.07Å^3 and for 900 °C annealed samples are a = 5.226Å, c = 11.437Å and V = 312.37Å^3. Unit cell volume calculated for ASP samples is slightly high because of the broadness of the peaks as compared to the standard JCPDS card no. 29:0351. Samples annealed at ~600 and 900 °C show slightly higher crystalline behaviour than ASP one, which are shown in Figure 4.1(b) and (c), respectively.

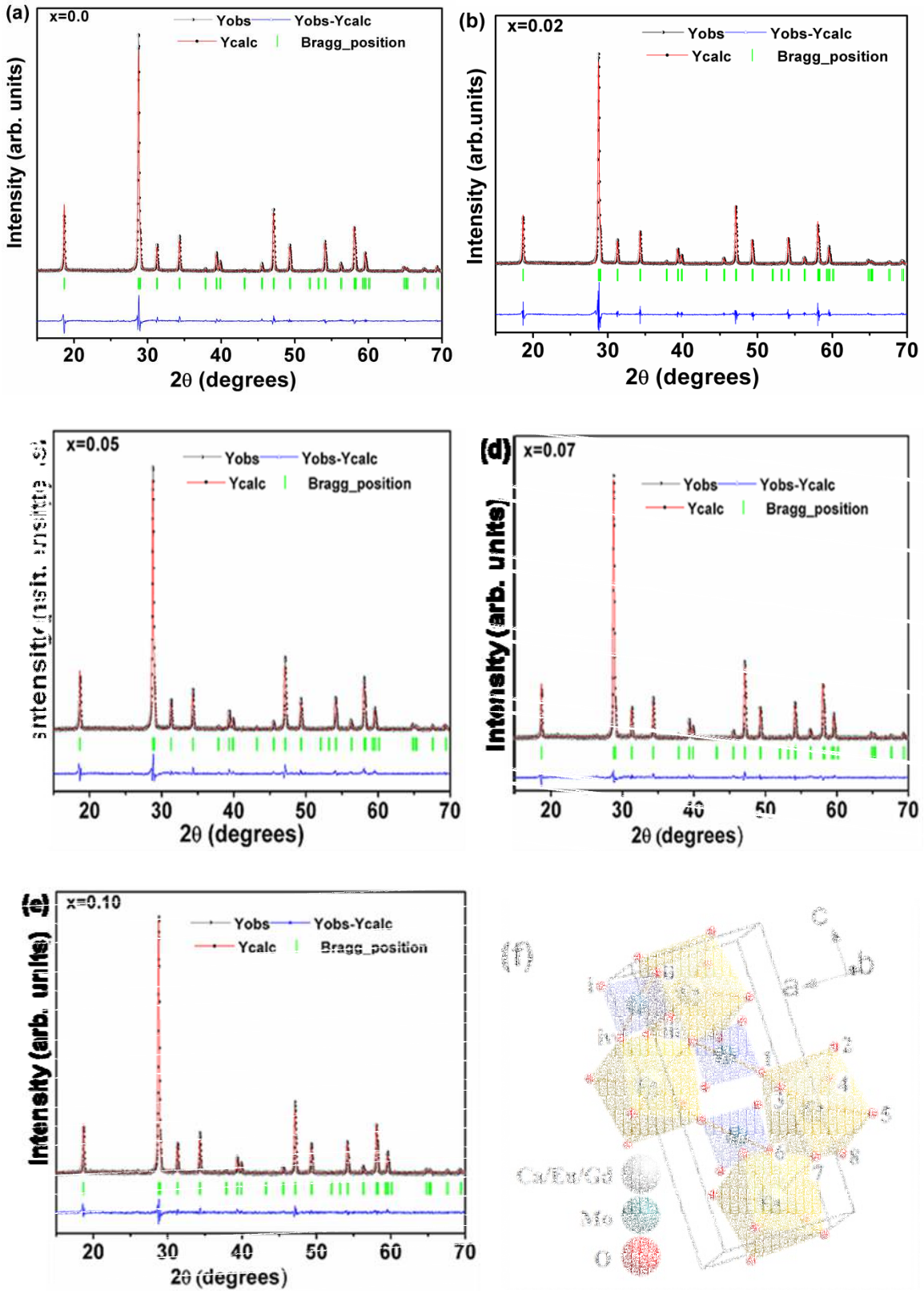

Figure 4.2: (a), (b), (c), (d) and (e) Rietveld plot of 0, 2, 5, 7 and 10 at.% Gd^{3+} co-doped $CaMoO_4$:Eu samples annealed at 900 ^oC and (f) simplified polyhedral representation of Gd^{3+} co-doped $CaMoO_4$:Eu having both $[CaO_8]$ and $[MoO_4]$ clusters.

The average crystallite size of the samples was calculated by using Scherrer formula as given in equation (3.1).

Average crystallite size determined using the Scherrer formula for the 2 at.% Gd^{3+}co-doped $CaMoO_4$:Eu of ASP, 600 and 900 ^oC annealed samples are found to be ~33, 48 and 61 nm, respectively. Average crystallite size of the samples annealed at ~600 and 900 ^oC is found to increase with the Gd^{3+} doping concentration. Structure refinement of Gd^{3+} (0, 2, 5 7 and 10 at.%) co-doped $CaMoO_4$:Eu samples annealed at ~600 and 900 ^oC was carried out using *FullProf* software [Carvajal, J. R.]. The peak profiles were modelled using Pseudo-Voigt function while background was described in terms of a six coefficient polynomial. R_{wp} (weighted-pattern factor) and S (goodness-of-fit) parameters were used as numerical criteria of the quality of fit to experimental diffraction data. Rietveld refinement patterns of Gd^{3+} (0, 2, 5, 7 and 10 at.%) co-doped $CaMoO_4$:Eu, for 900 ^oC are shown in Figure 4.2 (a-e). The Wyckoff positions of atoms based on space group $I4_{1/a}$ (88) and Z = 4 (number of $CaMoO_4$ formula units per unit cell) in $CaMoO_4$ unit cell are: [Parchur, et al.(2011b)]

Ca: (4b: 0, ¼, 5/8)

Mo: (4a: 0, 1/4/ 1/8)

O: (16f: x, y, z)

The Bragg reflections, difference in observed and calculated intensity are shown in figure itself. Moreover refinement patterns of Gd^{3+} (0, 2, 5, 7 and 10 at.%) co-doped samples of $CaMoO_4$:Eu annealed at 600 ^oC are shown in Figure 4.3(a)-(e). The crystal structure and symmetry resembled to that of its simplified 3D polyhedral representation are shown in Figure 4.2(f), which demonstrates the presence of high inversion symmetry in the lattice. As $CaMoO_4$ belong to the derivative of ABO_4 (A = Ca, Ba, Sr, Pb and B = Mo, W) with tetragonal scheelite structure having body centred inversion symmetry. A and B sites show S_4 point symmetry while its crystal structure comprises of two building block units namely, Eu/Gd/CaO_8 polyhedra and MoO_4 tetrahedra, respectively. In c direction, Eu/Gd/CaO_8 polyhedron shares four of its edges with four other Eu/Gd/CaO_8 polyhedrons through oxygen atoms. Oxygen atoms are sharing co-ordination among Eu/Gd/CaO_8 polyhedron and MoO_4 tetrahedron, respectively.

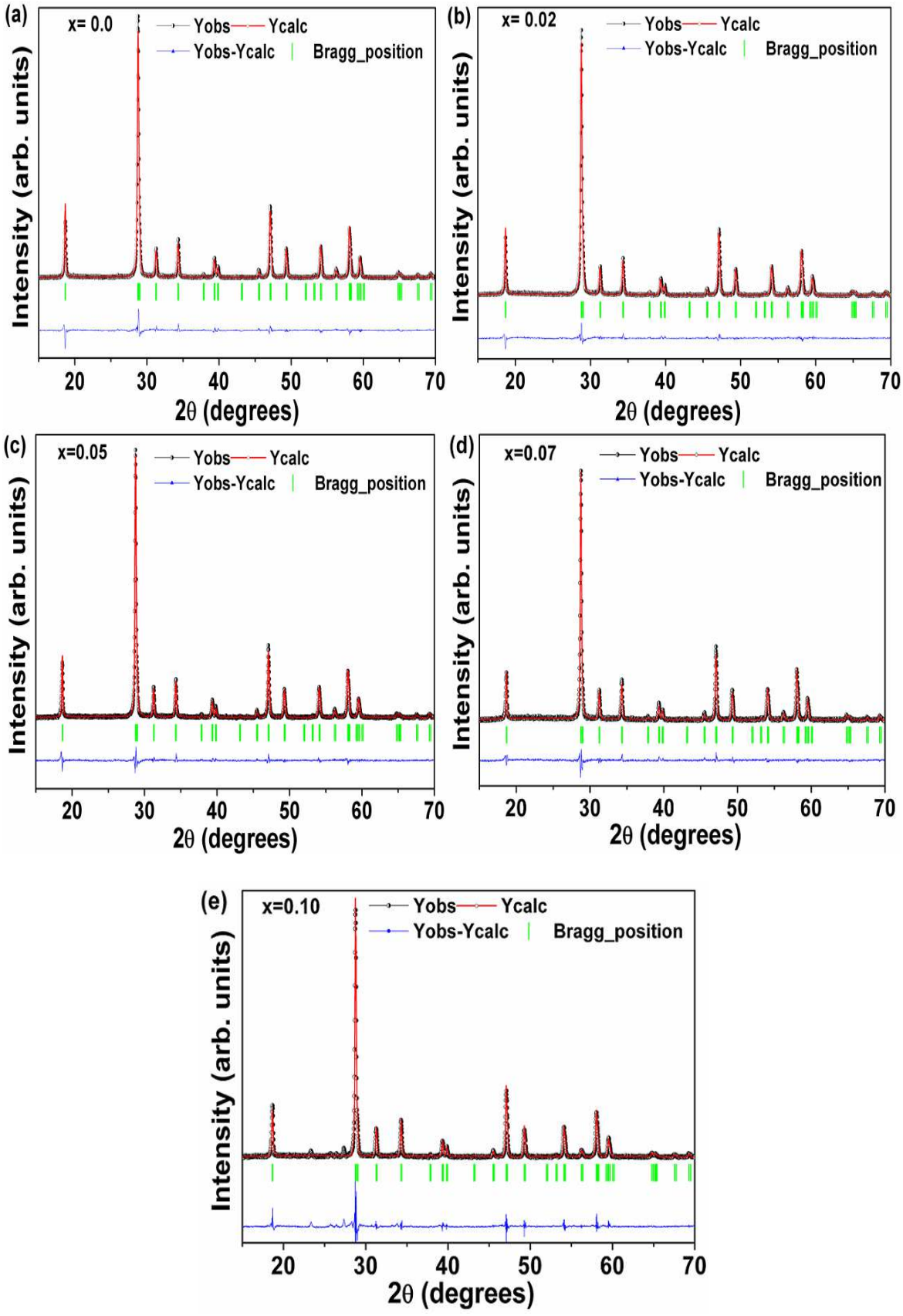

Figure 4.3: (a)- (e) Rietveld plots of Gd^{3+}(0, 2, 5, 7 and 10 at.%) co-doped $CaMoO_4$:Eu annealed at 600 ^oC.

Observed lattice parameters after Rietveld refinement, cell volume and average crystallite size for 600 and 900 ^oC samples for Gd^{3+} (0, 2, 5, 7 and 10 at.%) co-doped $CaMoO_4$:Eu samples are listed in Table 4.1.

Table 4.1: Calculated values of *a, c, V* and *D* for Gd^{3+} (0, 2, 5, 7 and 10 at %) co-doped $CaMoO_4$:Eu at 600 ^oC and 900 ^oC.

	600 ^oC				900 ^oC			
Gd^{3+}	*a*	*c*	*V*	*D*	*a*	*c*	*V*	*D*
0	5.224(2)	11.446(5)	312.11(19)	38	5.224(2)	11.439(4)	312.14(18)	59
2	5.223(2)	11.437(5)	311.97(02)	48	5.225(2)	11.434(3)	312.15(16)	61
5	5.226(2)	11.440(5)	312.28(02)	52	5.227(2)	11.437(5)	312.37(22)	62
7	5.226(2)	11.433(5)	312.25(19)	54	5.227(2)	11.431(4)	312.31(17)	71
10	5.226(2)	11.442(5)	312.16(21)	57	5.227(2)	11.4295(5)	312.27(19)	69

It is found that the cell volume slightly increases after Gd^{3+} incorporation in $CaMoO_4$:Eu for 900 ^oC annealed samples in comparison to samples annealed at 600 ^oC. This is may be due to ionic radii mismatch of Ca^{2+} ion as compared to Gd^{3+}/Eu^{3+}. Ionic radii of Eu^{3+} (1.07Å) and Gd^{3+} (1.07Å) are similar to Ca^{2+} (1.12Å) based on 8 coordination number (CN) [CaO_8] and Mo^{6+} has ionic radius of 0.42 Å in [MoO_4]. Therefore, Eu^{3+} and Gd^{3+} are supposed to occupy Ca^{2+} sites in spite of charge imbalance [Parchur, et al.(2011b), Shanon (1976)]. The micro-strain has been calculated for Gd^{3+} co-doped $CaMoO_4$ for ASP, 600 and 900 ^oC annealed samples using Williamson- Hall formula which has given as: [Kar, et al. (2010)]

$$\frac{\beta_{hkl}\cos\theta}{\lambda} = \frac{1}{D_{hkl}} + (\varepsilon_{hkl})\frac{\sin\theta}{\lambda} \qquad (4.2)$$

where β_{hkl} is the full width at half maximum (*FWHM*) of X-ray patterns, θ, the Bragg's diffraction angles, λ, the wavelength of X-ray, D_{hkl}, the effective crystallite size and ε_{hkl}

is the micro-strain. The instrumental broadening (ε_{ins}) is removed by using Si standard. Micro-strain is calculated for 0, 5 and 10 at.% Gd^{3+} doped $CaMoO_4$ and the values are found to be ~0.014, 0.0017, 0.0027 for ASP while ~0.0016, 0.0023 and ~0.0029 for 900 ^oC annealed samples, respectively. It has been inferred from the strain data that it increases with increase in Gd^{3+}concentration. Positive slope value ε_{hkl} indicates the presence of tensile strain acting on the system [Kar and Patra (2012)]. Dutta, et al.(2013) have reported recently the variation in strain (0.001-0.003) in Dy^{3+} doped $CaMoO_4$. It is found that strain increases with Dy^{3+} concentration, and being relaxed by co-doping of K^+ ions in $CaMoO_4$.

It is observed that pattern intensity of Gd^{3+} co-doped $CaMoO_4$:Eu is slightly less than $CaMoO_4$:Eu samples, which is due to defects created on Gd^{3+} co-doped $CaMoO_4$:Eu. Extra phases demonstrate the solubility limit of $Gd^{3+}$and Eu^{3+} ions in host lattice. It expected that up to 2 at.% of Eu^{3+} and up to 10 at.% Gd^{3+} charge compensation occurs for Ca^{2+} and oxygen ion vacancies. In the present study, nanophosphor is synthesized without any charge compensation of ions. The crystal structure are still consistent with scheelite phase with Gd^{3+} content up to 10 at.% for 600 and 900 ^oC annealed samples. Charge loss may be compensated as Ca^{2+} vacancies (V_{Ca}''). The defect equation mechanism for the Ca^{2+} vacancies can be proposed as:

$$3Ca^{2+} \rightarrow 2Eu_{Ca}^{\bullet} + V_{Ca}''$$

and

$$3Ca^{2+} \rightarrow 2Gd_{Ca}^{\bullet} + V_{Ca}''$$

In other words two Eu^{3+} or two Gd^{3+} ions must replace three Ca^{2+} sites to maintain charge balance and hence one V_{Ca}'' is created. Ionic radii mismatch among the Ca^{2+}, Eu^{3+} and Gd^{3+} are supposed to be responsible for the vacancy generation of V_{Ca}'' and creation of other point defects in the lattice. Similar behaviour have been reported for Bi^{3+} co-doped $CaMoO_4$:5Eu^{3+}[Yan, et al.(2007)].

4.1.3.1.2 FTIR study

FTIR spectra of the ASP, 600 and 900 ^oC annealed samples of 5 at.% Gd^{3+} co-doped $CaMoO_4$:Eu in the range 4000 - 400 cm^{-1} are shown in the Figure 4.4. Infrared absorption spectra show the all expected vibrational modes of calcium molybdate, which confirms the phase purity of the materials. Group theory calculations show that there are

having 26 modes of vibrations (Raman and infrared) for scheelite type structure which can be represented as: [Rousseau, et al. (1981)]

$$\Gamma_{(\text{Raman + Infrared})} = 3A_g + 5A_u + 5B_g + 3B_u + 5E_g + 5E_u \quad (4.3)$$

where A_g, B_g and E_g are Raman-active modes. There are 13 Raman active modes observed for the $CaMoO_4$ which is represented by equation as:[Porto and Scott (1967)]

$$\Gamma_{(\text{Raman})} = 3A_g + 5B_g + 5E_g \quad (4.4)$$

and eight infra-red active modes which is given as: [Golubovic et al.(2006)]

$$\Gamma_{(\text{infrared})} = 4Au + 4Eu \quad (4.5)$$

Infrared bands at ~1652 and 3419 cm^{-1} correspond to bending and stretching vibrational modes of absorbed water molecules on the surface of nanoparticles [Luwang, et al.(2010)].

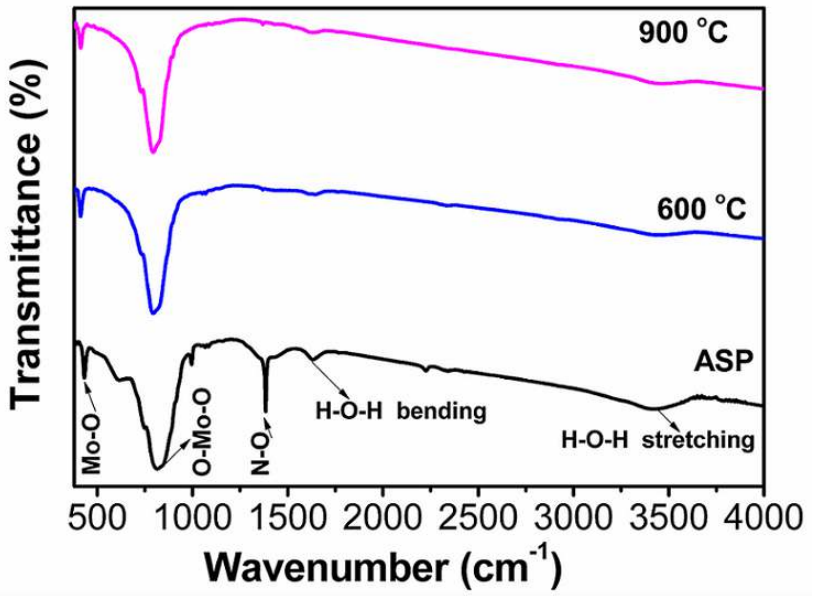

Figure 4.4: FTIR spectra of ASP, 600 and 900 °C annealed samples of 5 at.% Gd^{3+} co-doped $CaMoO_4$:Eu.

Observed absorption patterns intensity decreases as annealing temperature increases. Absorption peaks appearing at ~815 cm^{-1} is occurring due to the asymmetric stretching vibration of O-Mo-O vibration in MoO_4^{2-} tetrahedron, while peak at ~427 cm^{-1} occurs due to bending vibration of Mo-O of A_u mode [Lei and Yan (2008), Yang, et al.(2009)]. It observed that both O-Mo-O and Mo-O vibrations are slightly shifted towards lower wave number (~3-5 cm^{-1}) due to annealing the samples at 600 and 900 °C, which

infer the lattice expansion of $CaMoO_4$ host. The red shifts in Au mode of vibrations are responsible for lattice expansion in host. Band arises at ~1383 cm^{-1} demonstrates the presence of N-O modes of vibration of HNO_3 used in the sample preparation. Similar observation was reported in Tb^{3+} doped $CaMoO_4$ [Parchur, et al.(2012a)].

4.1.3.1.3 XPS study

The oxidation states of the constituent elements present in sample can be identified using XPS. Whole spectrum comprising of core BE levels of Ca, Mo, O, Eu/Gd is shown in Figure 4.5 obtained in the range of 0-1000 eV. XPS spectra of Ca, Mo and O core binding energy (BE) in ASP and 900 ^oC annealed samples of 0, 5 and 10 at.% Gd^{3+}co-doped $CaMoO_4$:Eu are shown in Figure 4.6 and Figure 4.7.

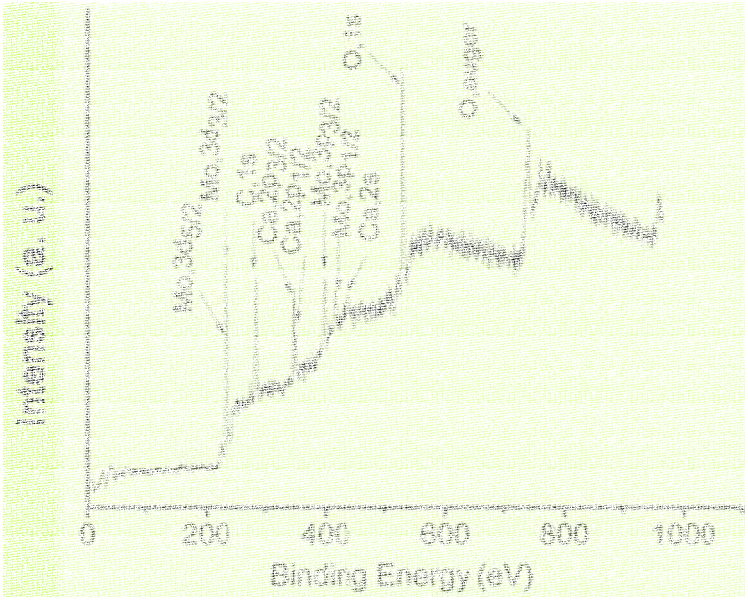

Figure 4.5: XPS spectrum of 5 at.% Gd^{3+} co-doped $CaMoO_4$:Eu annealed at 900 ^oC showing constituent elements involved in compositions.

Figure 4.6(a) (i)-(iii) shows the XPS spectrum of Ca (2*p*) for 0, 5 and 10 at.% Gd^{3+} co-doped $CaMoO_4$:Eu ASP samples. For Gd^{3+} free $CaMoO_4$:Eu sample, the peaks are corresponding to Ca (2*p*) having core BE ~346.84 ($2p_{3/2}$) and 350.39 eV ($2p_{1/2}$) and full width at half maximum (FWHM) ~1.7 and 2.0 eV. On increasing Gd^{3+} (5 and 10 at.%) co-doping concentration, there is slight changes in BE values to higher eV. Moreover, integrated intensity ratio of ($2p_{3/2}$) to ($2p_{1/2}$) (I_{Ca}) is found to be 1.76, 1.9 and 1.47 for 0, 5 and 10 at.% Gd^{3+} co-doping, respectively. On annealing the sample at 900 ^oC, there is slight decrease in BE of Ca($2p_{3/2}$) and Ca($2p_{1/2}$) by 0.25-0.47 eV for 0, 5 and 10 at.% Gd^{3+} co-doped $CaMoO_4$:Eu samples which is shown in Figure 4.6(b) (i)-(iii); and FWHM and

I_{Ca} does not change significantly within the limits of error bar. These results confirm 2+ oxidation state of Ca. Figure 4.6(c) (i) shows the peaks at ~232.64 and 235.77 eV, which correspond to the core BE of Mo($3d_{5/2}$) and Mo($3d_{3/2}$), respectively for ASP Gd^{3+} free $CaMoO_4$:Eu sample. Integrated intensity ratio of ($3d_{5/2}$) to ($3d_{3/2}$) (I_{Mo}) are found to be 1.36, 1.49 and 1.39 for 0, 5 and 10 at.% Gd^{3+} co-doping samples, respectively (Figure 4.6(c) (i)-(iii)).

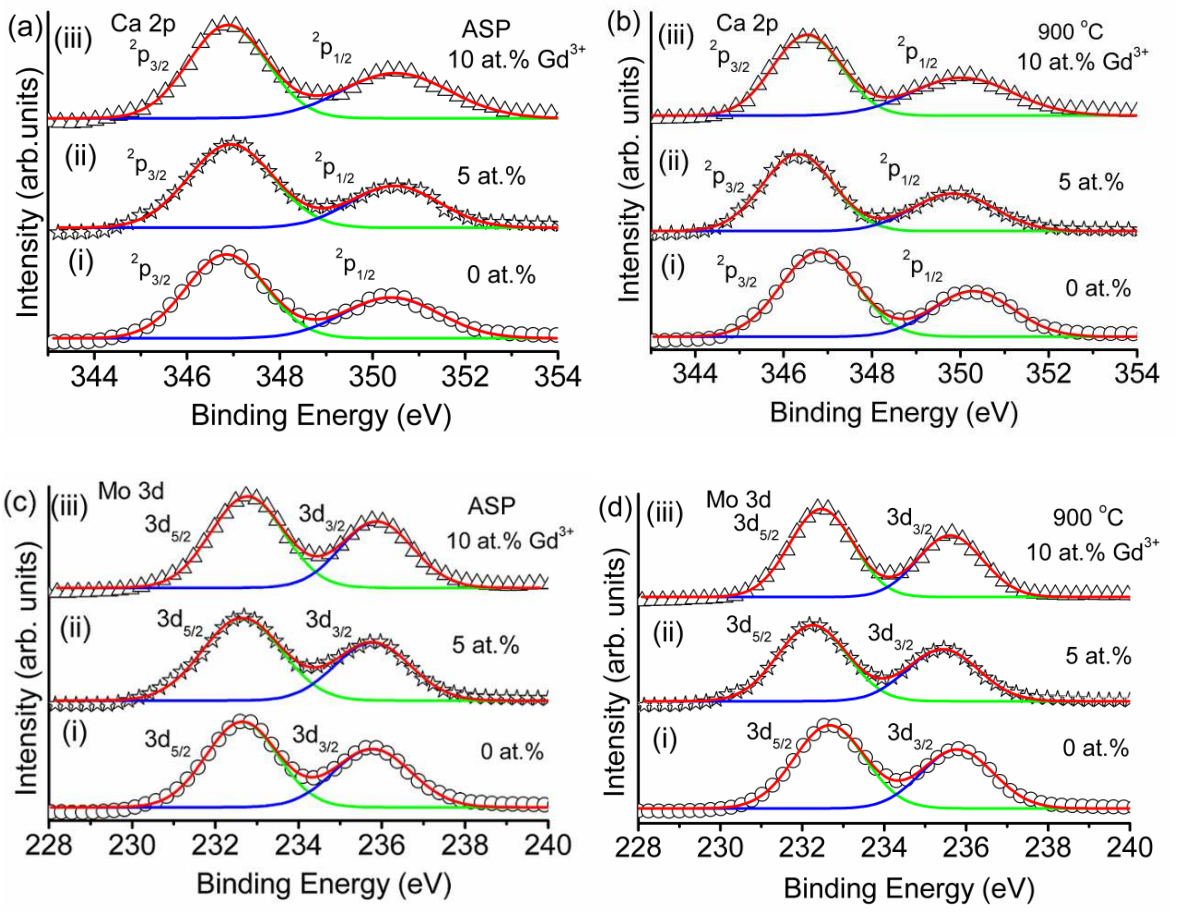

Figure 4.6: (a) to (d) XPS spectra of as-prepared and 900 °C annealed samples 0, 5 and 10 at.% Gd^{3+} co-doped $CaMoO_4$:Eu. Peaks corresponding to the core binding energies of individual elements viz, Ca and Mo.

There is no significant change in BE on Gd^{3+} co-doping. On annealing the samples at 900 °C, BE are slightly shifted to lower eV by 0.17 to 0.47 eV (Figure 4.6 (d) (i)-(iii)). Also, (I_{Mo}) found to be 1.39, 1.43 and 1.39 eV for 0, 5 and 10 at.% Gd^{3+} co-doping samples, respectively. The lack of any significant change in the $3d_{3/2}$-$3d_{5/2}$ BE in the Mo spectral region suggests that Mo ions remain in its Mo^{6+} state. Similar behaviour was supported in literatures for Ca-Bi-Mo oxide and for the molybdenum phosphate glass [Woo, et al.(2004), Khattak, et al.(1997)]. Notably the peaks for Gd^{3+} and Eu^{3+} fall on

~141-148 eV. So it is bit difficult to distinguish $Eu^{3+}(4d_{3/2})$ and $Gd^{3+}(4d)$. Peak at ~141.1 eV, which corresponds to $Eu^{3+}(4d_{3/2})$ and there having no peak at ~127.1 eV corresponding to $Eu^{2+}(4d_{5/2})$ is observed. This is confirmed that the high probability of Eu^{3+} is present in the sample. It is also confirmed from excitation/emission study (not shown). Moreover, small peaks at 141.4 and 146.2 eV correspond to $Gd(2p_{3/2})$ and $Gd(2p_{5/2})$, respectively[Singh, et al.(2014b), Zhou, et al.(2012)]. Typical XPS spectra showing core binding energy and intensity of Eu and Gd in 10 at.% ASP and 900 °C annealed Gd^{3+} co-doped $CaMoO_4$:Eu is shown in Figure 4.7 (a), (b).

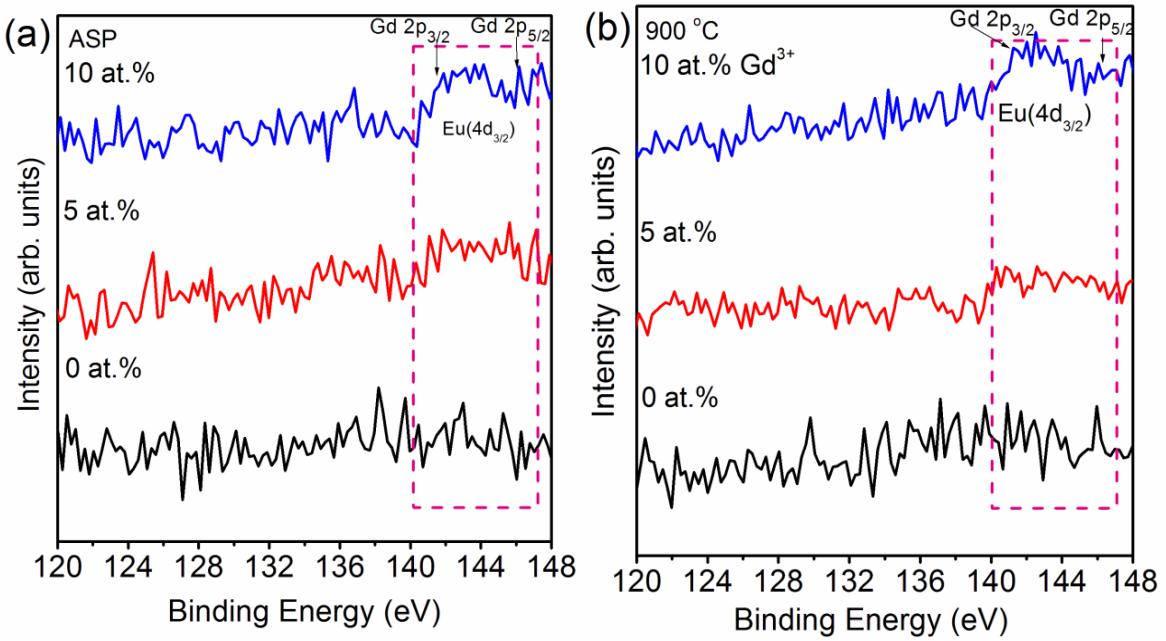

Figure 4.7: XPS spectra of Eu/Gd of (a) ASP and (b) 900 °C annealed, Gd^{3+} (0, 5 and 10 at.%) co-doped $CaMoO_4$:Eu.

Intensity of these peaks is very small for ASP and 900 °C annealed samples and improves with increase of Gd^{3+} concentration. It is may be due to presence of less no of Gd^{3+}/Eu^{3+} ions presents in the sample. In addition, O(1s) spectral regions have been used to obtain the information regarding the presence of oxygen vacancies present in the sample (Figure 4.8).

Peaks were deconvoluted using Gaussian function. In case of ASP Gd^{3+} free $CaMoO_4$:Eu sample, two peaks are well fitted at BE ~ 529.5 (P_1) and 531.6 eV (P_2) having FWHM ~1.8 and 1.82 eV, respectively. On increasing Gd^{3+} co-doping peak position slightly changes by ± 0.1-0.4 eV (Figure 4.8(a)).

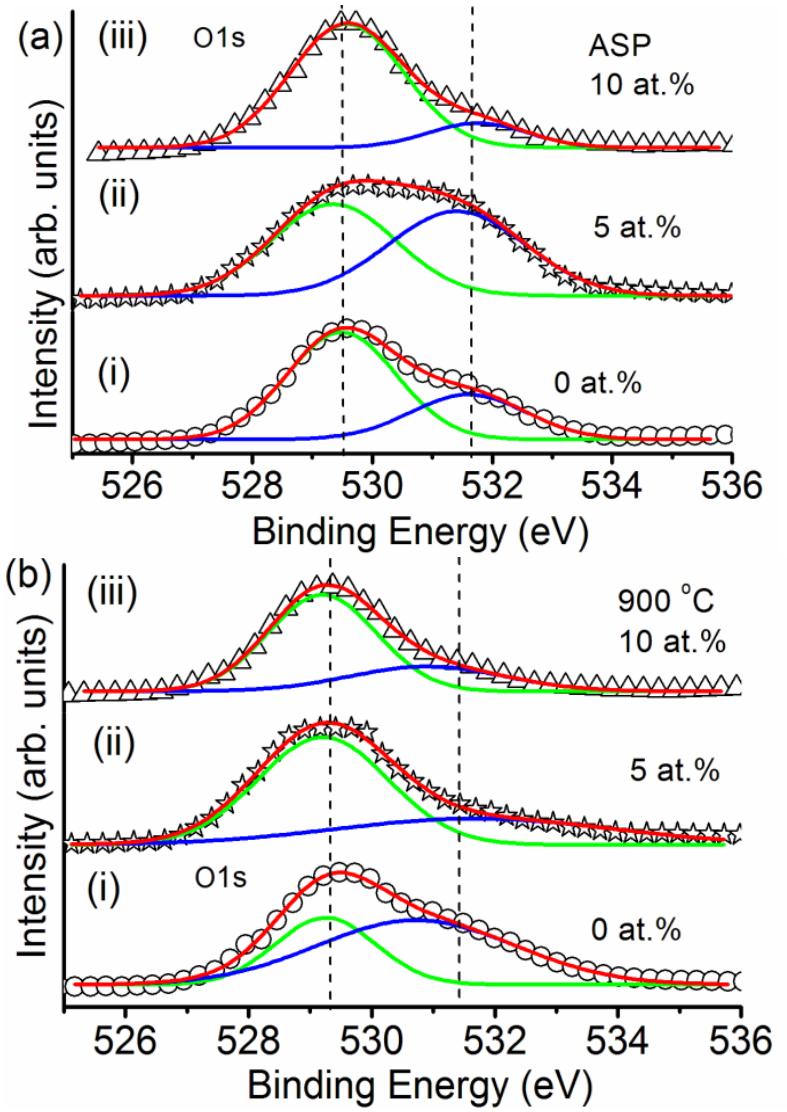

Figure 4.8: XPS spectra of O1s for (a) ASP and (b) 900 °C annealed, Gd^{3+} (0, 5 and 10 at.%) co-doped $CaMoO_4$:Eu.

Similar spectra are observed upon annealing the sample at 900 °C (Figure 4.8(b)). BE of the peaks is shifted to ~± 0.26-0.76 eV with respect to corresponding ASP samples. Overall peaks show asymmetric nature in higher BE side. Further relative area of P_2/P_1 of ASP and 900 °C annealed samples for 0, 5 and 10 at.% Gd^{3+}co-doped $CaMoO_4$:Eu provides an interesting features shown in Figure 4.9. This is may be due to the defects and of oxygen vacancies creation on behalf of non-isovalant dopant. There are few reports which indicate that high energy side of O(1s) peak arises due to hydroxyl groups –OH or other radicals on the sample surface as CO or CO_2 [Shah, et al.(2009)]. However, the asymmetric behaviour at high energy peak (~530.5 eV) in an O1s spectrum is signature of the presence of oxygen ion vacancy in the lattice [Parchur, et al. 2012(c)]. It can be suggested that oxygen vacancy decreases with annealing sample at high temperature.

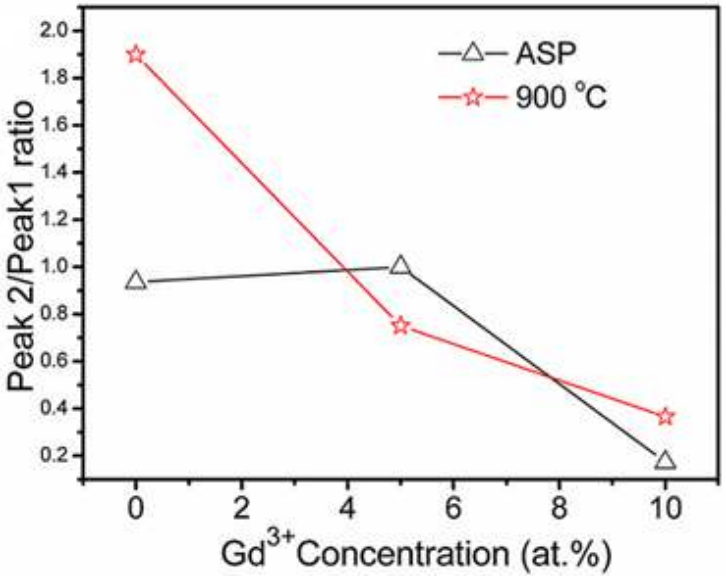

Figure 4.9: Variation of relative peak intensity of peak2 to peak1 of O1s spectra of 0, 5 and 10 at.% Gd^{3+} co-doped $CaMoO_4$:Eu for ASP and 900 °C annealed samples.

4.1.3.1.4 DT-TGA study

Thermal decomposition of ASP $CaMoO_4$:Eu in air has been studied by thermo gravimetric (TGA) and differential thermal analyses (DTA), shown in Figure 4.10. TG curve shows two distinct stages of weight loss. First weight loss (~2%) step is observed between 55-140 °C, which is attributed to the removal of residual water molecules absorbed on the sample surface.

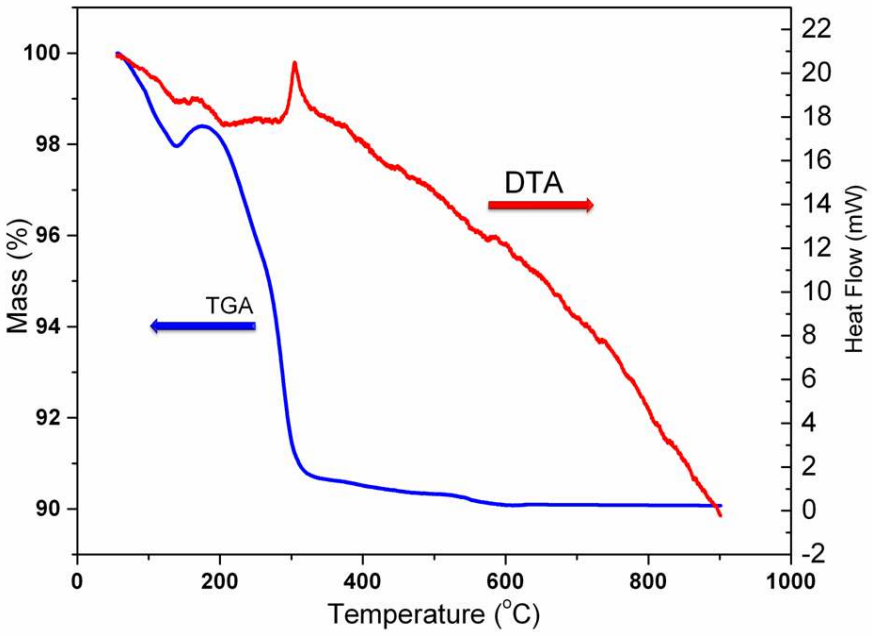

Figure 4.10: TG-DTA curves of as-prepared precursor for $CaMoO_4$:Eu in synthetic air.

The second weight loss (10%) is in the temperature range 140-600 ^oC accompanied by an exothermic peak at 305 in DTA curve which may be due to the further combustion of organic matrices like hydrocarbons, carbonates and nitrates. Moreover, weight loss after ~600 ^oC becomes constant and thereafter no significant loss has been observed upto 900^oC. This demonstrates that combustion and decomposition of all organic constituent precursors in the samples have been completed below 600 ^oC.

4.1.3.1.5 SEM and TEM studies

Morphological aspect of the $CaMoO_4$:Eu nanophosphors of ASP, 600 and 900 ^oC are investigated by taking the SEM and TEM micrographs. Typical SEM morphology of $CaMoO_4$:Eu nanophosphors of ASP, 600 and 900 ^oC heated samples are shown in Figure 4.11(a), (b) and (c), respectively. The scale bar indicated on each figure corresponds to size of 100 nm. In ASP, there are agglomerated particles in which one particle contains many small crystallites. Each crystallite has 30-40 nm size. In 600 ^oC, particles are spherical in shape and smallest particle has size of 50-60 nm. In 900 ^oC, bigger aggregates of spherical particles are obtained and smallest particle has size of 350-360 nm.

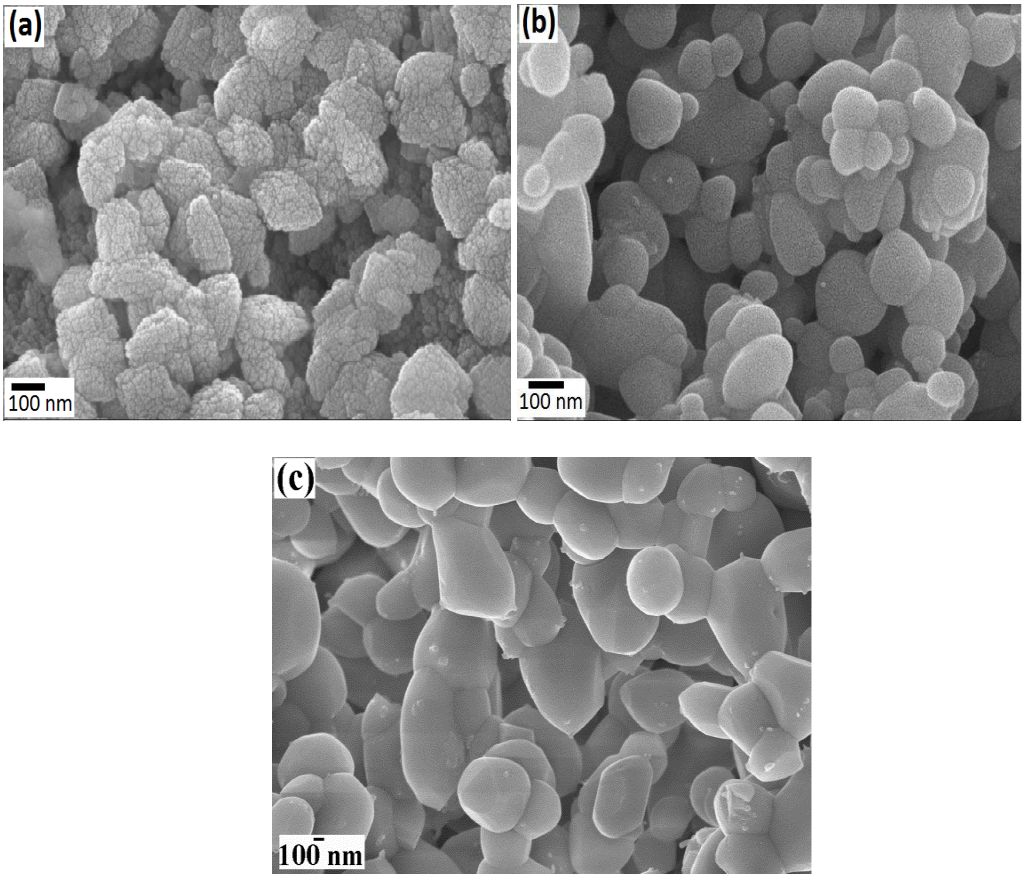

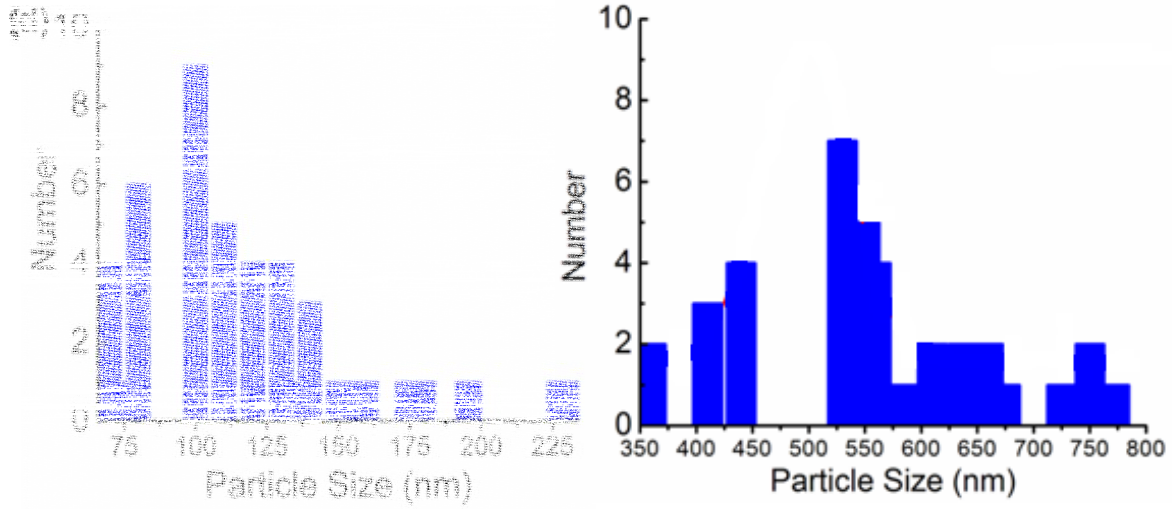

Figure 4.11: FE-SEM images of micro-spherical particles $CaMoO_4$:Eu for (a) as-prepared (b) 600 (c) annealed at 900 °C (d) particle size distribution for 600 °C and (e) for 900 °C annealed samples.

It is observed that as annealing temperature increase, the particle size increases. Particle size distribution histograms for 600 (Figure 4.11(b)) and 900 °C (Figure 4.11(c)) annealed samples are presented in Figure 4.11 (d) and Figure 4.11 (e), respectively. Mean diameters of the particles for 600 and 900 °C annealed $CaMoO_4$:Eu is found to be ~100 and ~500 nm.

Typical TEM micrographs of ASP 5 at.% Gd^{3+} co-doped $CaMoO_4$:Eu are shown in Figure 4.12(a). Many crystallites form agglomerated particle. This is similar to SEM observation. HRTEM of 5 at.% Gd^{3+} co-doped $CaMoO_4$:Eu at 900 °C is used to calculate *d* spacing and corresponding (*hkl*) plane, which is shown in Figure 4.12 (c). It confirms that maximum growth of the crystal have been taken along the (101) plane and d_{101} = 4.5 Å. To check the growth direction of planes and their corresponding *d* spacing, we have analysed by taking various plane spots in HRTEM, which is shown in Figure 4.12 (d) marked as (i), (ii), (iii) and (iv). From this, it is infered that in most of the cases i.e. at (i), (ii) and (iii) spots, *d* spacing is same as marked in Figure 4.12(c). For region marked as (iv), some crystal growth takes place in (004) planes with spacing having 2.77 Å which is shown in Figure 4.12 (e). Energy dispersive spectra (EDS) of ASP 5 at.% Gd^{3+}co-doped $CaMoO_4$:Eu is shown in the Figure 4.12 (b). EDS analysis reveals the presence of the most intense peaks of Mo along with calcium (Ca), oxygen (O), europium (Eu), gadolinium (Gd) and Cu peaks. Presence of Cu peaks in the EDS spectra are manifestation from the copper micrometer grids. Moreover, no other impurities were pronounced indicating that Gd^{3+}co-

doped $CaMoO_4$:Eu phosphors are chemically pure in composition via auto combustion route.

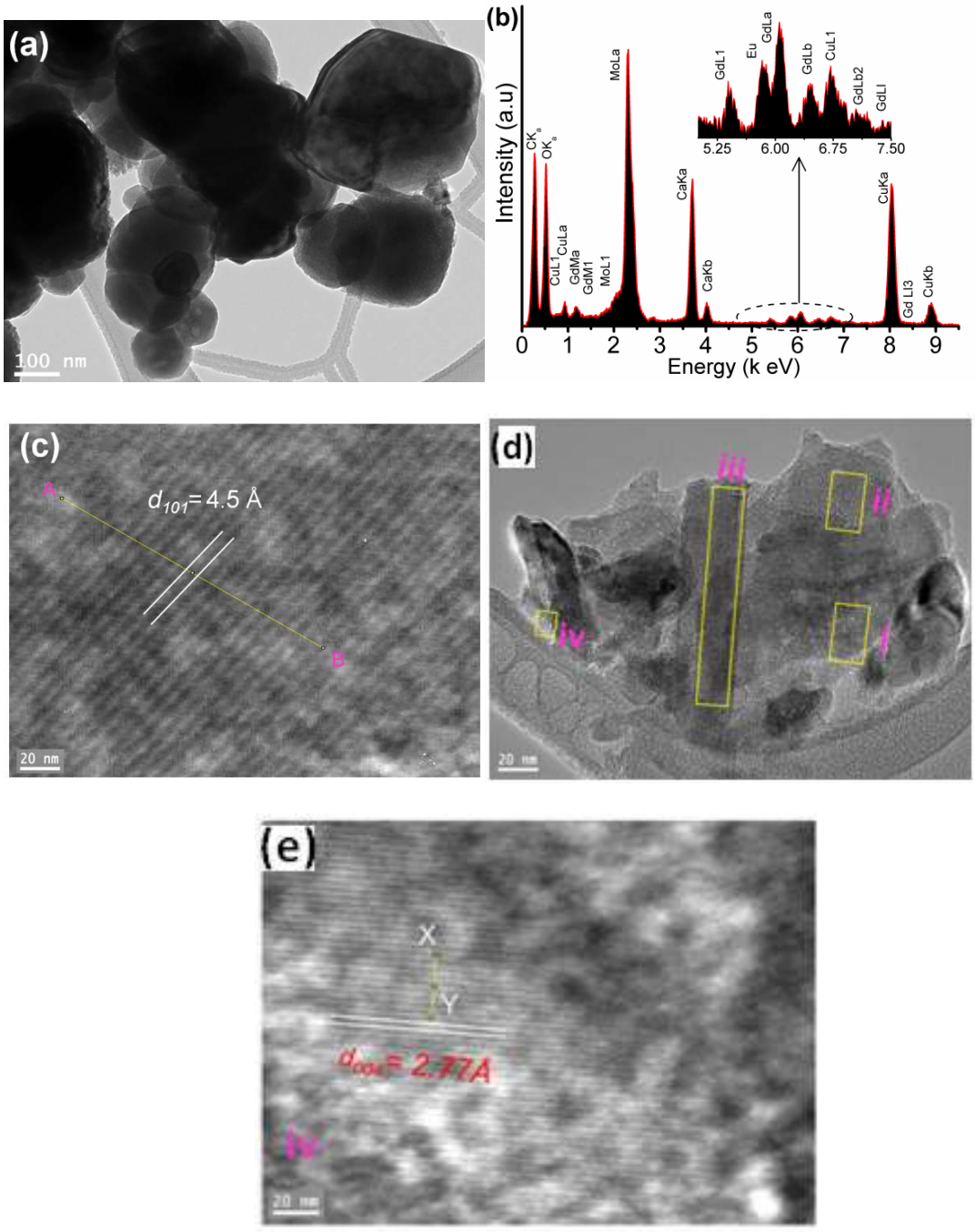

Figure 4.12: (a) TEM and (b) shows the elemental composition of a large area of ASP 5at.% Gd^{3+} co-doped $CaMoO_4$:Eu nanophosphors, which is verified by the presence of Ca, Mo, Eu and Gd peaks. Cu peak comes from the Copper grid used for the electron microscopy analysis and (c), (d) and (e) HRTEM images for region (i), (ii), (iii) and (iv) of 5at.% Gd^{3+} co-doped $CaMoO_4$:Eu at 900 ^oC. Scale bar is given under 20 nm.

4.1.4 Conclusion

Highly crystalline Gd^{3+} (0, 2, 5, 7 and 10 at. %) co-doped $CaMoO_4$:Eu nanoparticles are synthesized under facile auto-combustion route. In order to get the higher crystallinity, ASP sample is heated up to 600 and 900 ^oC. The tetragonal scheelite phase having space group $I4_1/a$ and Z = 4 is found. Extra peaks in XRD patterns are found in case of ASP and 600 ^oC and these are not there in 900 ^oC. FTIR spectrum shows the bands at ~815 cm^{-1} and 427 cm^{-1}, which are due to asymmetric stretching and bending vibrations of O-Mo-O of MoO_4^{2-} tetrahedron, respectively. From XPS study, Ca is found to be +2 oxidation state; while Mo, Eu and Gd are found to be +6, +3 and +3 oxidation states, respectively. Core binding energy peak at ~141.1 eV corresponds to $Eu^{3+}(4d_{3/2})$. No peak at ~127.1 eV which corresponds to $Eu^{2+}(4d_{5/2})$ is observed. This supports the high probability of Eu^{3+} present in the samples. The particle size increases with annealing.

Part-2

4.2 Enhanced Photoluminescence in $CaMoO_4:Eu^{3+}$ by Gd^{3+} co-doping

4.2.1 Introduction

Lanthanide (Ln^{3+}) doped molybdates and tungustates having Scheelite type (ABO_4, A = Ca, Sr, Mg and Ba; B = Mo and W) have been extensively studied by the scientific community as a multifunctional materials because of its diverse and prominent applications in acousto- optic filters, solid state lasers, white light emitting diodes (w-LED), scintillations, fluorescent lamps, solar cell, electrolyte material for solid oxide fuel cells and catalysis [Longo, et al.(2011), Marques, et al.(2010), Van der Ende, et al.(2009)]. $CaMoO_4$ reflects its intriguing features having high melting points (1445-1480 ^oC), refractive index (1.98), photoelectron yield (9%), non-hygroscopic and higher thermal, chemical and mechanical stabilities [Annenkov, et al. (2008)]. It can give a blue to green light under UV excitation depending on particle size. In recent years, calcium molybdate has been extensively studied as a potential phosphor because of higher chemical stability as compared to other fluoride ($NaYF_4$ and/or $BaYF_5$) and oxide materials. Many reports have been published on the photoluminescence of calcium molybdate ($CaMoO_4$) doped with different lanthanide ions [Parchur, et al.(2011a), Parchur et al.(2012a) , Raju, et al.(2012), Jin, et al.(2008)]. Nowadays, much attention is focused on enhancing the luminescent intensity of phosphors. Besides the energy transfer from sensitizer to activator, like Ce^{3+} to Tb^{3+}, another way to improve the efficiency of phosphors is a quantum cutting process [Zhong, et al.(2010)]. Rare earth ions such as Sm^{3+}, Eu^{3+}, Tb^{3+}, Er^{3+}, Tm^{3+} and Ho^{3+} have been used as luminescence centers because they have their abundant energy levels for radiative transition, and some are suitable for direct pumping by UV/Vis or NIR laser diode [Cavalli, et al.(2010), Mahlik, et al.(2013), Jin, et al.(2011), Chung, et al.(2012)]. Currently, Gd^{3+} based material can be effectively used as a contrast agent in MRI for medical diagnosis and marker in bio-labeling/bio-imaging [Ren, et al.(2012)]. Recently, Eu^{3+} and Er^{3+}/Yb^{3+} doped $GdVO_4$ show a 9potentiality as a luminomagntic under UV excitation[Gupta, et al.(2011), Yin, et al.(2012)]. Also rare earth doped $NaGdF_4$ has been proposed as a potential bimodal imaging phosphors [Park and Hyeon (2009), Shivakumar, et al.(2009)]. However rigorous low efficiency of these nonomaterials stringently confined their pervading applications. Consequently, it will be of great interest and worthy of pursuit to significantly increase the emission intensity of phosphors in order to deploy their

potential applications. At these limited conditions for using rare earth ions as emitters in real devices, a better understanding of the excitation and quenching mechanisms should be investigated in details to optimize their optical properties.

A single-component white-light phosphor is normally produced by co-doping a sensitizer and an activator into the same host matrix. A few significant investigations have been done to improve the luminescent properties of $CaMoO_4$ phosphor by co-doping other metal ions. The energy transfer mechanism from a sensitizer to an activator such as Eu^{2+}/Mn^{2+}, Ce^{3+}/Mn^{2+}, and Ce^{3+}/Eu^{2+} couples has been investigated in many inorganic hosts, and an effective resonance-type multi polar interaction has been verified in $NaSr_4(BO_3)_3$: Ce^{3+}, Mn^{2+}, Na-$Ba_4(BO_3)_3$: Ce^{3+}, Mn^{2+}, $Sr_3Sc(PO_4)_3$: Eu^{2+}, Mn^{2+}, $Sr_3B_2O_6$: Ce^{3+}, Eu^{2+}, and so on. Moreover, some single-phase phosphors, such as $Ca_{10}K(PO_4)_7$:Eu^{2+}, Mn^{2+}, Ca_9Y-$(PO_4)_7$: Eu^{2+}, Mn^{2+}, $Ca_9Y(PO_4)_7$: Ce^{3+}, Eu^{2+}, and $Ca_9Y(PO_4)_7$: Ce^{3+}, Mn^{2+}, are used to improve the emission intensity for *n*-UV LED (light emitting diode) applications [Zhang, et al.(2011), Zhang and Seo (2010), Guo, et al.(2013), Chang and Chen (2007), Huang et al.2010 (a), Huang, et al.(2011), Huang, et al. 2010 (b)]. Yan, et al. (2007) have reported the improvement in luminescence intensity of 3 orders in magnitude of $CaMoO_4$:5Eu^{3+} on Bi^{3+} co-doping. Also an improvement in photo-luminescence intensity has been reported with co-doping of charge compensators such as Li^+, K^+, Na^+ and Bi^{3+} in phosphors or with SiO_2 coating over particle of phosphor. In this direction, non-raditaive rates are reduced by either charge compensation, improve crystallinity or extent of decrease of surface dangling bonds/OH bonds by shell from inner core phosphor [Xie, et al.(2009), Liu, et al.(2007), Ningthoujam (2012)]. However, the energy transfer between Eu^{3+}/Gd^{3+} in nanophosphors, which can be synthesized through auto-combustion route, is rarely investigated. Gd^{3+} ion is using as co-dopant in Eu^{3+}, $Tb^{3+}$and Dy^{3+} and in many other hosts in order to improve luminescence [Romanowski, et al.(2002), Li, et al.(2007)]. The reason for improvement in luminescence of Ln^{3+} is not understood till date because emission peak at 310 nm for Gd^{3+} is not fully matching with absorption band of Ln^{3+}[Zhong, et al.(2010), Sahu, et al.(2012)]. The energy transfer in case of up-conversion luminescence is generally different from that of down-conversion. There are following energy transfer processes in down conversion luminescence: [Zhong, et al.(2010), Ningthoujam (2012)]

(i) Resonance type in which emission band for sensitizer (S) is matched with absorption band of activator (A) (i.e., S $\rightarrow$ A),

(ii) Non-radiative energy transfer from higher excited state of M to A,

(iii) Quantum cutting by a two/more-step energy transfer from M to A,

(iv) Increase of absorption cross-section of M and followed by energy transfer from M to A.

Here M represents the phosphor. Upon excitation at any wavelength, the electrons go to the excited state. However, the excited state is either the excited energy levels of M (from electronic or band transition) or simply no excited energy level of M. Excitation energy is usually more than the minimum absorption energy of A.

In this Chapter, we have prepared Gd^{3+} (0, 2, 5, 7 and 10 at.%) co-doped $CaMoO_4$:Eu nanoparticles via efficient auto-combustion technique. For the optimal Eu^{3+} concentration (2 at.% in this study), prominently enhanced red emission of Eu^{3+} is obtained for the as-prepared, 600 and 900^oC annealed samples by addition of Gd^{3+} co-doping instead of varying Eu^{3+} concentration. The photoluminescence property of $CaMoO_4$:Eu has been investigated in detail for ASP, 600 and 900 ^oC annealed samples. It may be a potential suitable red phosphor material which is bottleneck for the advancement in white LED at much lower cost.

4.2.2 Experimental details

Gd^{3+} (0, 2, 5, 7 and 10 at.%) co-doped $CaMoO_4$:Eu nanoparticles were prepared via facile auto-combustion technique. As-prepared sample (ASP) was annealed at 600 and 900 ^oC for 4 hours each [Singh, et al. 2014(b)]. Concentration of Eu^{3+} is fixed at 2 at.%. Samples show tetragonal phase. Crystallinity increases with increase of annealing temperature. As-prepared sample, 600 and 900 ^oC annealed samples are considered as ASP, 600 ^oC and 900 ^oC, respectively. The UV-Vis absorption spectra were measured using Perkin-Elmer Lambda-40 spectrophotometer in the range 190-600 nm. The UV/Vis absorption spectra were measured on a Perkin-Elmer Lambda-40 spectrophotometer in the range 190–600 nm, with the sample contained in a 1 cm^3 stoppered quartz cell of 1 cm path length. Photoluminescence excitation spectra of the samples were recorded using Hitachi F-4500 spectrometer attached with a 150 W Xe lamp as a source having spectral resolution of 3 nm. Photoluminescence spectra were studied by a 266 nm pulsed Nd-YAG laser (Spitlight 600, Innolas, Germany) source. Photoluminescence decay was recorded with Edinburg instrument F-920 equipped with 100 W μs flash xenon lamp as the excitation source. All measurements were performed at room temperature.

4.2.3 Results and Discussion

4.2.3.1 Absorption studies

The calculation of associated optical band gap energy for ASP, 600 and 900 °C was calculated using model proposed by Wood and Tauc [Wood and Tauc (1972)]. According to this model, optical band gap follows the relation as:

$$\alpha h\nu \propto (h\nu - E_g)^n \qquad (4.6)$$

where α is the absorbance, h is the Planck constant, ν is the frequency, E_g is the optical band gap of nanomaterial. The exponent n is the constant which can have values n = 1/2, 2, 3/2 or 3 depending on the way of transitions, i.e., direct allowed, indirect allowed, direct forbidden and indirect forbidden transitions, respectively. The literature supports that molybdates have an optical absorption governed by direct electronic transitions [Longo, et al.(2011), Marques, et al.(2010)]. Typical energy gap calculation of 5 at.% Gd^{3+} co-doped $CaMoO_4$:Eu for ASP, 600 and 900 °C samples from absorption spectra is shown in Figure 4.13 and estimated values are found to be ~5.07, 4.71 and 4.68 eV, respectively. Decrease in energy band gap of host is related to increase of particle size upon annealing [Marques, et al.(2010), Singh, et al.2014a, Thongtem, et al.(2010)].

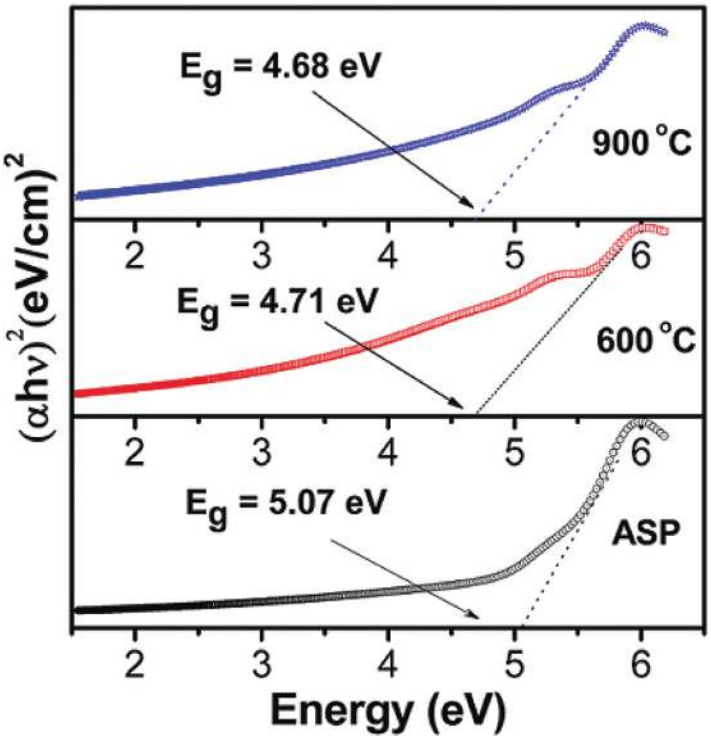

Figure 4.13: $(\alpha h\nu)^2$ *vs.* $h\nu$ for ASP, 600 and 900 °C annealed samples of 5 at.% Gd^{3+} co-doped $CaMoO_4$:Eu in absorption spectra.

4.2.3.2 Photoluminescence study

4.2.3.2.1 Excitation study

Figure 4.14(a) shows excitation spectra of ASP sample of Gd^{3+} (0 and 10 at.%) co-doped $CaMoO_4$:Eu, monitoring the emission wavelength at 613 nm. The broad peak at 220-350 nm and sharp peaks with low intensity between 350-550 nm are observed. These broad peaks arises due to overlap of Eu-O and Mo-O charge transfers (CT) [Hou, et al.(2009), Lei and Yan (2008), Yaiphaba, et al.(2010)]. Peaks at 247 and 272 nm are assigned to be Eu-O and Mo-O CT band, respectively [Parchur, et al.(2011a)]. The sharp excitation peaks due to intra-configurationally *f-f* transitions of Gd^{3+} ions were reported at 255 nm ($^8S_{7/2} \rightarrow {}^6D_{9/2}$), 275 nm ($^8S_{7/2} \rightarrow {}^6I_{11/2}$) and 277 nm ($^8S_{7/2} \rightarrow {}^6I_{9/2}$) [Zhong, et al. (2010)]. While peaks at ~362, 376, 382, 396, 412, 466 and 532 nm are assigned to $^7F_0 \rightarrow {}^5D_4$, $^7F_0 \rightarrow {}^5G_3$, $^7F_0 \rightarrow {}^5G_4$, $^7F_0 \rightarrow {}^5L_6$, $^7F_0 \rightarrow {}^5D_3$, $^7F_0 \rightarrow {}^5D_2$ and $^7F_0 \rightarrow {}^5D_1$, respectively of intra-configurationally *f-f* transitions of Eu^{3+} ions.

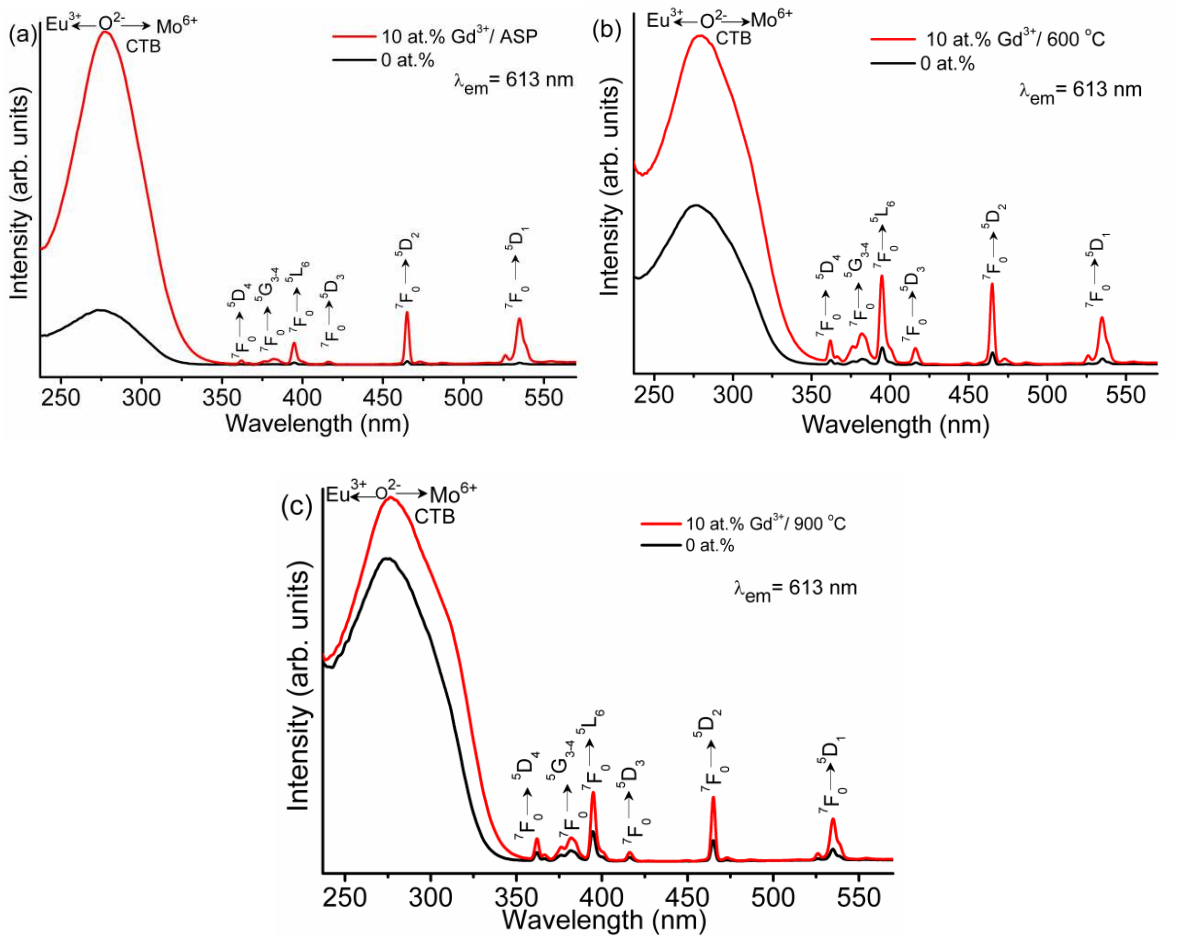

Figure 4.14: Excitation spectra of Gd^{3+} (0 and 10 at.%) co-doped $CaMoO_4$:Eu nanoparticles: (a) ASP, (b) 600 and (c) 900 ^oC annealed samples (monitoring emission at 613 nm).

The absorption peaks for Gd^{3+} are overlapping with Eu-O and Mo-O CTB. On monitoring emission wavelength of Eu^{3+} at 613 nm, there are strong broad peak in 220-350 nm and weak peaks in 350-550 nm. This confirms an efficient energy transfer from Gd^{3+}/Mo-O/Eu-O to Eu^{3+}. It is ascribed from the excitation spectra that intensity of Gd^{3+}/Mo-O CT absorption band increases for higher concentration of Gd^{3+} (10 at.%) co-doped samples than the Gd^{3+} free samples. Here, concentrations of Mo^{6+} and Eu^{3+} are fixed in all samples. Increase of intensity in 320-250 nm with increasing Gd^{3+} indicates that there is energy transfer from Gd^{3+} to Eu^{3+} by possible processes (ii-iv) mentioned in Introduction section. Here process (i) will be minimum since there is least overlapping of emission band at 313 nm ($^6P_{7/2}\rightarrow{}^8S_{7/2}$) for Gd^{3+} with absorption band of Eu^{3+}. Similar reports on effects of Gd^{3+} has been reported on the Tb^{3+} activated $Ca_2Gd_8Si_6O_{26}$ nanophosphors [Raju, et al.(2011)]. It is worthy to mention from the Figure 4.14(a) that the Gd/Mo-O CT band around 275 nm peak is more symmetrical for Gd^{3+} free $CaMoO_4$:Eu than 10 at.% Gd^{3+} co-doped $CaMoO_4$:Eu. More broadening and asymmetricity have been observed for the 10 at.% Gd^{3+} co-doped $CaMoO_4$:Eu samples annealed at 600 and 900 ^oC than Gd^{3+} free sample of $CaMoO_4$:Eu. The intensities variation of Gd/Mo-O CT band at around 275 nm were higher than that of ($^7L_0\rightarrow{}^5L_6$) transition at ~395 nm; and the intensity of $^7F_0\rightarrow{}^5D_2$ at 465 nm is higher than that of 395 ($^7L_0\rightarrow{}^5L_6$) of Eu^{3+} ions is higher than that of 532 nm ($^7F_0\rightarrow{}^5D_1$) (i.e., Gd/Mo-O CT band > 465 nm > 395 nm > 532 nm) for ASP samples. Figure 4.14(b) and (c) show the excitation spectra of 600 and 900 ^oC annealed samples monitoring the emission wavelength at 613 nm. Peaks are similar to that of the ASP samples. For 600 and 900 ^oC annealed samples, it is observed that in the longer wavelength region, the intensity of peak ($^7L_0\rightarrow{}^5L_6$) at 396 nm peak is higher than that of 465 nm ($^7F_0\rightarrow{}^5D_2$) and 532 nm ($^7F_0\rightarrow{}^5D_1$). As annealing temperature increases, it is observed that Eu-O/Mo-O CT band maximum is shifted towards lower energy side. It is related to increase in covalent character in Eu-O/Mo-O [Ningthoujam, et al.(2009), Igarashi, et al.(2000)].

4.2.3.2.2 Emission Study

Emission spectra of Gd^{3+} (Gd^{3+} = 0, 2, 5, 7 and 10 at.%) co-doped $CaMoO_4$:Eu (ASP, 600 and 900 ^oC annealed samples) are shown in Figure 4.15 under 266 nm Nd-YAG laser excitation. The spectrum shows a strong emission peak at 613 nm. It is observed that incorporation of Gd^{3+} ion in $CaMoO_4$:Eu does not have effect on shape of spectra but

changes the PL intensity enormously. Emission spectra comprise of five characteristics emission lines of Eu^{3+} which are originated from $^5D_1 \rightarrow {}^7F_1$ and $^5D_0 \rightarrow {}^7F_j$ (j = 1, 2 , 3, 4). The emission peaks at ~590 ($^5D_0 \rightarrow {}^7F_1$) and 613 nm ($^5D_0 \rightarrow {}^7F_2$) are assigned to magnetic and electric dipole transitions of Eu^{3+}, respectively. The $^5D_0 \rightarrow {}^7F_2$ transition is hypersensitive, found to be dominant over all peaks in the spectra. It is found that emission intensity of Eu^{3+} increases with Gd^{3+} up to 2 at.% Gd^{3+} for ASP samples and then decreases. This may be due to the surface defects and concentration quenching effect. PL intensity increases up to 7 at.% and 10 at.% Gd^{3+} for 600 and 900 °C annealed samples, respectively. This may be due to the extent of reduction of nonradiative rates come from the surface dangling bonds, water molecule adsorbed at surface and removal of -NO and -CH groups upon annealing at higher temperature.

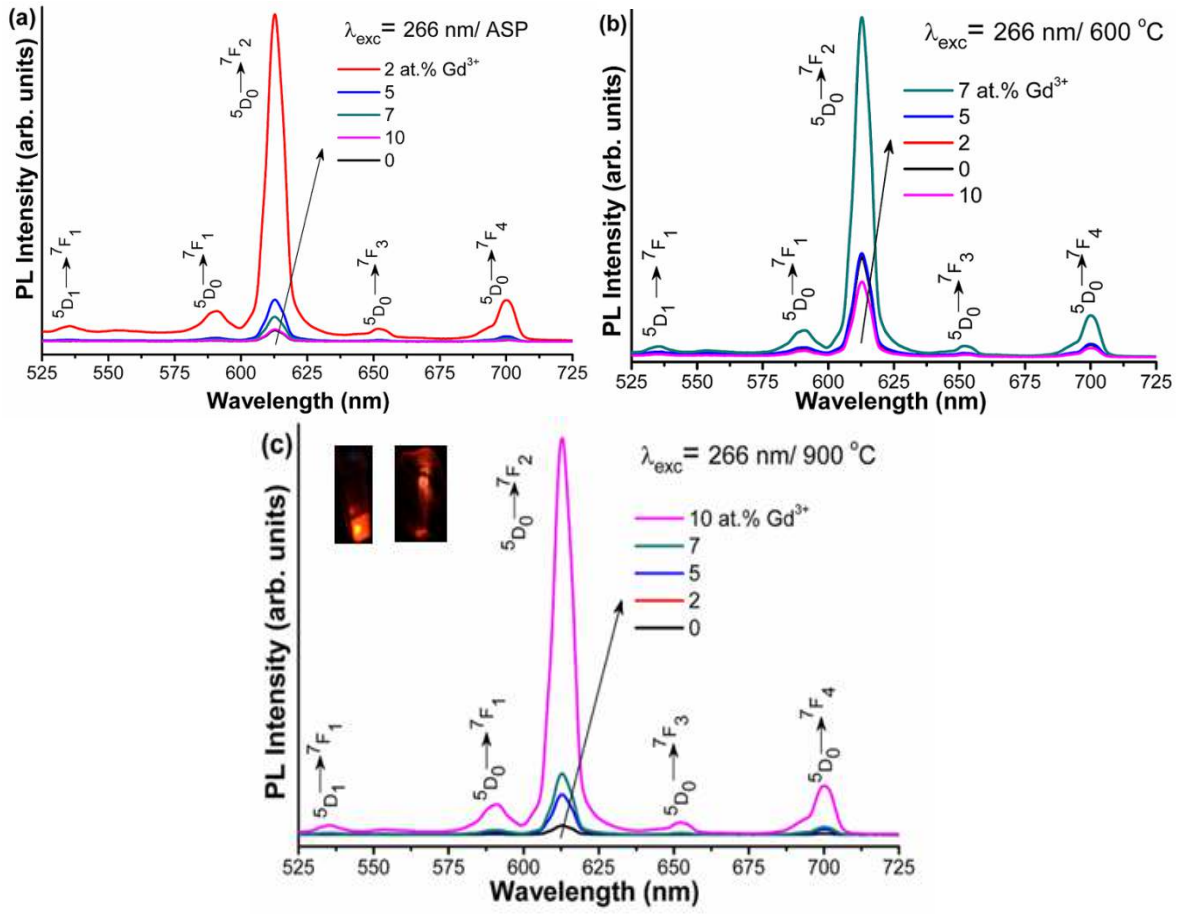

Figure 4.15: Luminescence spectra of Gd^{3+}(0, 2, 5, 7 and 10 at.%) co-doped $CaMoO_4$:Eu nanoparticles: (a) ASP (b) 600 (c) 900 °C (inset show the digital photographs of powder sample and polymer film under 266 nm laser excitation of 2 at.% Gd^{3+} co-doped $CaMoO_4$:Eu.

In order to compare the emission intensities of electric and magnetic dipole transitions, the Gaussian function is used to fit the curve. The magnetic and electric dipole transitions are fitted by relation as;

$$I = I_B + \frac{A_1}{w_1\sqrt{\pi/2}} e^{2\left[(\lambda-\lambda_{c1})^2/w_1^2\right]} + \frac{A_2}{w_2\sqrt{\pi/2}} e^{2\left[(\lambda-\lambda_{c2})^2/w_2^2\right]} \quad (4.7)$$

where I is the intensity, I_B is the background intensity, A is the area of the corresponding peaks, w is the *FWHM*, λ is the wavelength, while λ_c is the average value to the assigned transitions. These peaks are fitted well in the range 580-600 nm for magnetic and 600-630 nm for electric dipole transitions, respectively. Typical fitting data of magnetic to electric dipole transitions of 5 at.% Gd^{3+} co-doped $CaMoO_4$:Eu sample annealed at 600 ^oC under ~266 nm excitation is shown in the Figure 4.16. It is well fitted with value of χ^2= 0.9967. Values of fitting parameters are marked in the figure itself.

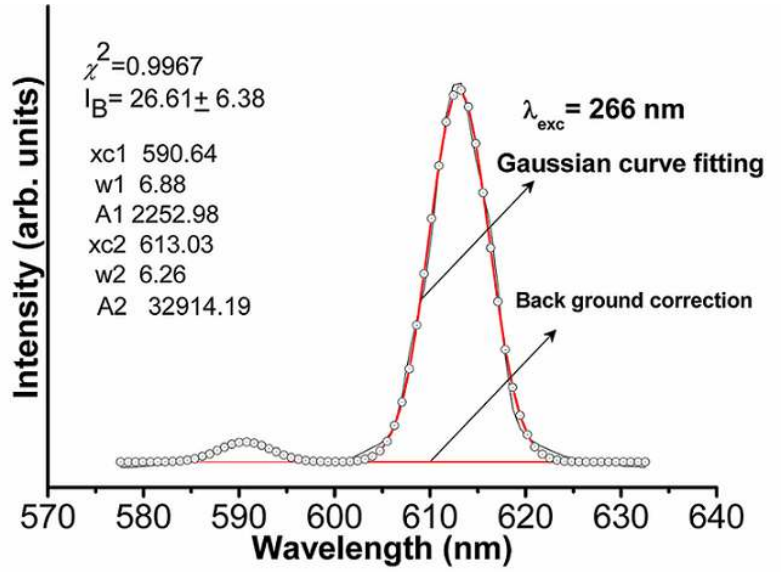

Figure 4.16: Typical fitting of magnetic and electronic dipole transitions of 5 at.% Gd^{3+} co-doped $CaMoO_4$:Eu heated at 600 ^oC.

The detailed analyses of peak position of magnetic $^5D_0 \rightarrow {}^7F_1$ and electric dipole transition $^5D_0 \rightarrow {}^7F_2$ and FWHM of Gd^{3+} (0, 2, 5, 7 and 10 at.%) co-doped $CaMoO_4$:Eu for ASP, 600 and 900 ^oC heated samples are listed in Table 4.2. Emission peaks corresponding to magnetic and electric dipoles after Gaussian profile curve fitting to assigned transition do not shift at a great extent but FWHM values of the peaks decreases gradually for ~600 and 900 ^oC heated samples of Gd^{3+} (0, 2, 5, 7 and 10 at.%) co-doped $CaMoO_4$:Eu. Figure 4.17(a) shows the variation of intensities (integrated area under curve) for ASP, 600 and

900 °C annealed samples of Gd^{3+} (0, 2, 5, 7 and 10 at.%) co-doped $CaMoO_4$:Eu. Slight improvement in peak profile intensity for 600 °C is observed as compared to ASP one while peak intensities (integrated area under the curve) is significantly high for the 900 °C samples.

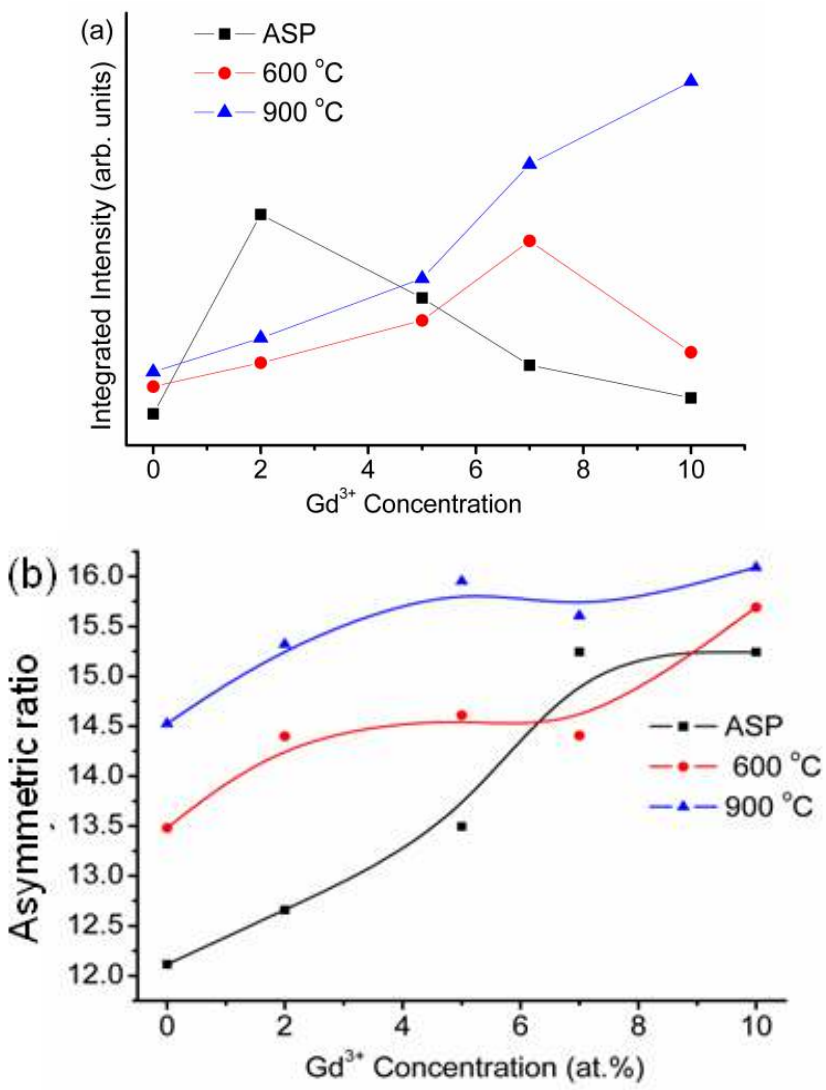

Figure 4.17: (a) Photoluminescence intensity variation of Gd^{3+} co-doped (0, 2, 5, 7 and 10 at.%) $CaMoO_4$:Eu of ASP, 600 and 900 °C annealed samples and (b) Asymmetric ratio A_{21} variation of Gd^{3+} co-doped (0, 2, 5, 7 and 10 at.%) concentration of $CaMoO_4$:Eu of ASP, 600 and 900 °C annealed samples.

Comparatively low luminescence intensity is observed for 600 °C because at lower temperature, the particle having ample surface to volume ratio, which leads to sufficient amount of non radiative transitions. In case of 900 °C annealed samples, particles have lower surface to volume ratio which results in decrease of nonradiative transitions and hence the improved photoluminescence is observed. Similar behaviour is reported for Eu^{3+}

doped $GdVO_4$ system [Singh, et al.(2008)]. Asymmetric environment of Eu^{3+} ion in host lattice can be calculated by integrated intensities ratio of electric ($^5D_0 \rightarrow {}^7F_2$) to magnetic ($^5D_0 \rightarrow {}^7F_1$) dipole transitions. It is termed as asymmetric ratio represented as $A_{21,}$ where subscript '2' and '1' refer transitions of $^5D_0$ to ^7F_j, j = 2 and 1, respectively.

Table 4.2: Peak positions of the magnetic dipole transition $^5D_0 \rightarrow {}^7F_1$ and electric dipole transition $^5D_0 \rightarrow {}^7F_2$ and their respective FWHM of ASP, 600 and 900 ^oC heated samples of Gd^{3+} (Gd^{3+} = 0, 2, 5, 7 and 10 at.%) co-doped $CaMoO_4$:Eu. λ_{exc} = 266 nm.

Gd^{3+} (at.%)	ASP		600 ^oC		900 ^oC	
	($^5D_0 \rightarrow {}^7F_1$) /w (nm)	($^5D_0 \rightarrow {}^7F_2$) /w (nm)	($^5D_0 \rightarrow {}^7F_1$) /w (nm)	($^5D_0 \rightarrow {}^7F_2$) /w (nm)	($^5D_0 \rightarrow {}^7F_1$) /w (nm)	($^5D_0 \rightarrow {}^7F_2$) /w (nm)
0	589.42/8.01	613.04/6.29	590.09/6.79	612.99/6.26	590.25/6.81	613.03/6.25
2	589.07/8.61	612.98/6.38	590.22/6.82	612.98/6.31	590.27/6.83	612.99/6.25
5	590.25/7.23	612.92/6.36	589.92/6.88	613.02/6.26	590.38/6.54	612.99/6.23
7	589.94/7.16	612.96/6.35	590.03/7.17	612.98/6.35	590.26/6.67	612.99/6.23
10	590.03/7.05	612.96/6.33	589.99/7.04	613.01/6.26	590.35/6.66	612.97/6.26

In a site with inversion symmetry, the $^5D_0 \rightarrow {}^7F_1$ transition is dominant while in a site without inversion symmetry, the $^5D_0 \rightarrow {}^7F_2$ transition is dominating [Shang, et al.(2011)]. A_{21} is calculated as;

$$A_{21} = \frac{\int_{600}^{630} I_2 d\lambda}{\int_{580}^{600} I_1 d\lambda} \tag{4.8}$$

where I_2 and I_1 are the intensities of electric and magnetic dipole transitions, respectively calculated after background correction subjected to the peaks under Gaussian fit and λ is the wavelength. Photoluminescence spectra reveal that maximum intensity occurs at 613 nm $^5D_0 \rightarrow {}^7F_2$ hypersensitive electric dipole transition which is highly sensitive to the asymmetric environment around Eu^{3+}. Hence the variation in peak intensity of electric dipole transitions with respect to Gd^{3+} concentration under ~266 nm excitation is studied. A_{21} value increases upon annealing the sample at 600 and 900 ^oC as compared to ASP (Figure 4.17 (b)). A_{21} values for 5 at.% Gd^{3+} co-doped $CaMoO_4$:Eu in case of ASP, 600 and 900 ^oC annealed samples are found to be ~13.49, 14.60 and 15.95, respectively. In present study, maximal values of A_{21} are found up to ~16 under ~266 nm Nd: YAG laser

excitation. This higher value in A_{21} signifies that higher local disorder/distortion occur in the Gd^{3+} co-doped $CaMoO_4$:Eu host lattice and lattice distortion induces more odd-rank crystal field components such as $4f^5 5d$ mixed into the electronic transition levels of $4f^6$ of Eu^{3+}after Gd^{3+} addition and hence enhances the photoluminescence intensity significantly. Similar trend of A_{21} value has been reported in literature for Eu^{3+} doped (Li, $Na)_2(Gd_4MoO_4)_7$ under ~466 nm lamp excitation and for Bis-β diketonate lanthanide complexes [Thomas, et al.(2009), Shi et al.(2013)]. Parchur, et.al (2011a) has reported the asymmetric ratio of Eu^{3+} under different lamp excitation source and found the value to be in the range ~2-10 with Eu^{3+} concentration in $CaMoO_4$:Eu. Asymmetric ratio calculated for ASP, 600 and 900 ^oC under ~266 nm excitation with Gd^{3+} (0, 2, 5, 7 and 10 at.%) co-doped $CaMoO_4$:Eu samples is shown in the Figure 4.17(b).

Figure 4.18 shows the schematic diagram of energy levels in Gd^{3+} co-doped $CaMoO_4$:Eu. Band gap of $CaMoO_4$ is ~4.6-5.1 eV (Figure 4.13), which is comparable with Eu-O charge transfer band (4.8-5.1 eV = 240-260 nm) and greater than Gd^{3+} absorption band at ~3.96 eV.

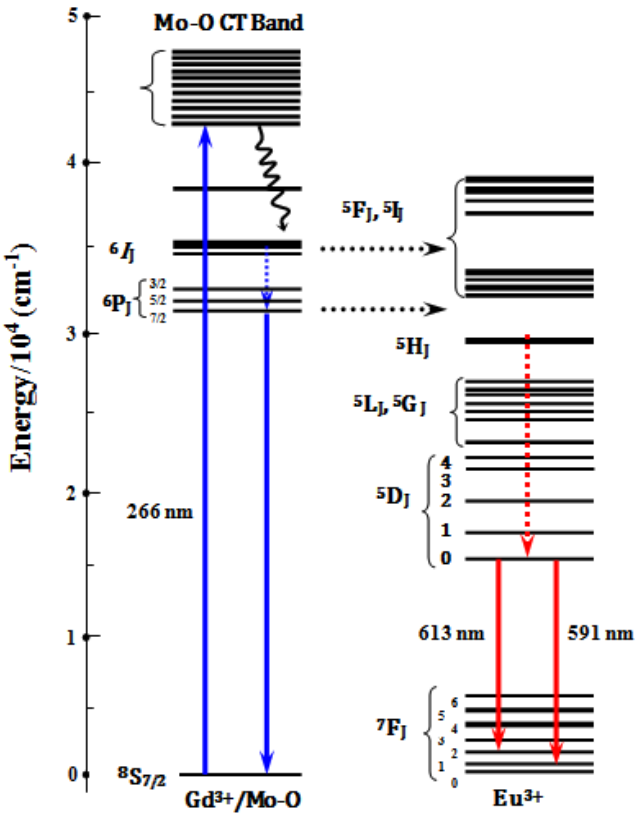

Figure 4.18: Schematic energy level diagram for transfer process between Gd^{3+}/MoO_4^{2-} and Eu^{3+} ions in $CaMoO_4$.

However, there is weak absorption band in 240-255 nm for Gd^{3+}[Zhong, et al. (2010)]. Because of decrease in surface defect or capping ligands on particles surface, the band gap of the samples slightly decreases on annealing at 600 and 900 ^oC, which is also supported by UV-Visible absorption measurement (Figure 4.13). After excitation at ~266 nm (4.66 eV), the excited electrons go from Mo-O CT band/Gd^{3+} band (^6I_J) to the excited state of Eu^{3+} ion and relax to ground state levels of Eu^{3+} ion with strong emission at red color regions.

4.2.3.2.3 Solvents effect on emission intensity and polymer film studies

ASP sample of 2 at.% Gd^{3+} co-doped $CaMoO_4$:Eu was proved to be useful for the easy dispersion of nanoparticles in polar solvents like water, ethanol, methanol, di-methyl sulphoxide (DMSO) and ethylene glycol (EG). For a typical dispersion of the nanoparticles, 10 mg of ASP sample of 2 at.% Gd^{3+} co-doped $CaMoO_4$:Eu, is dispersed in 10 ml of water, ethanol, methanol, DMSO and EG followed by ultra-sonication. Well dispersed nanoparticles in polar medium could be verified up to ~1-2 months without settlement. This may be due to hydrogen bonding between MoO_4^{2-} unit and/or functional group of polar solvent.

Figure 4.19 shows the emission spectra of re-dispersed 2 at.% Gd^{3+} co-doped $CaMoO_4$:Eu in different solvents viz. water, ethanol, methanol, DMSO and EG under 266 nm laser excitation. For the entire solvents, f-f transitions of Eu^{3+} are well observed and the intensity of $^5D_0 \rightarrow {}^7F_2$ transition (red) is found to be more significant.

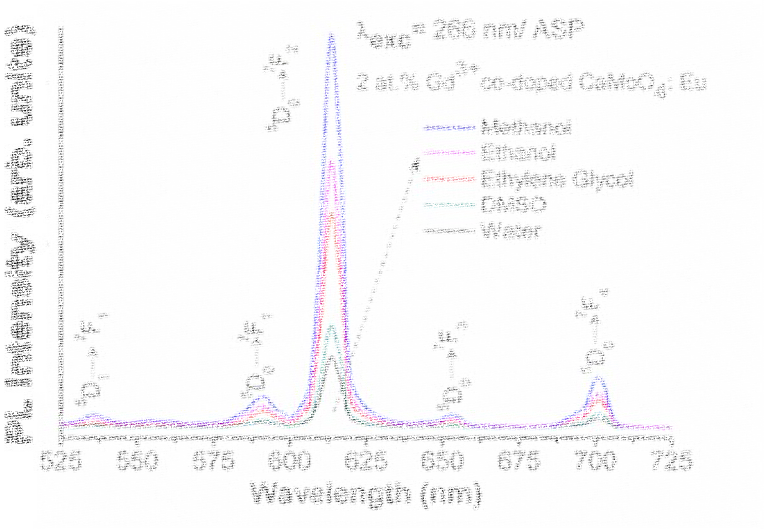

Figure 4.19: PL emission intensities spectra in different solvents viz. water, ethanol, methanol, DMSO and EG of ASP 2 at.% Gd^{3+}co-doped $CaMoO_4$:Eu (inset show the digital photographs of dispersed solution in EG before and after irradiation under 266 nm Nd-YAG source excitation).

The order of intensity is found to be highest for methanol amongst the other solvents. The polarity index of methanol is having minimal among the other solvents [C. Reichardt and T. Welton (2011)]. High polarity index has the large number of quenching sites and thus, solvent with higher polarity will have the lower luminescence intensity. It is observed that peak positions of magnetic and electric dipole transitions are unaffected after dispersion of the nanoparticles into these polar solvents. Asymmetric ratio A_{21} obtained for these solvents is not altered significantly as compared to powdered samples. For a typical thin film processing of 2 at.% Gd^{3+} co-doped $CaMoO_4$:Eu, 5 mg of ASP sample is mixed with 5 ml of distilled water. After that 0.5 g of PVA and 5 ml of ethanol is added. For the uniform dispersion of the sample, it is ultrasonicated for 30 minutes. This solution is poured into poly petri dish. It is kept for 2-3 days at room temperature for the drying purpose. In this way polymer films having thickness ~0.2-0.3 mm and diameter ~10 cm of 2 at.% Gd^{3+} co-doped $CaMoO_4$:Eu are prepared. In inset Figure 4.15(c), it is evident that film shows bright red under 266 nm laser excitation. Uniform brightness of thin film confirms the homogeneous distribution of the particles in the polymer matrix. PL spectrum of PVA thin film after incorporation of re-dispersed particles of ASP 2 at.% Gd^{3+}co-doped $CaMoO_4$:Eu at 266 nm laser excitation is shown in Figure 4.20. It is observed that emission intensities of ASP nanoparticles re-dispersed in water, ethanol, methanol, DMSO, EG and in PVA matrix are slightly less in comparison to powder samples. This is due to the less concentration of Eu^{3+} ion per unit volume of dispersion.

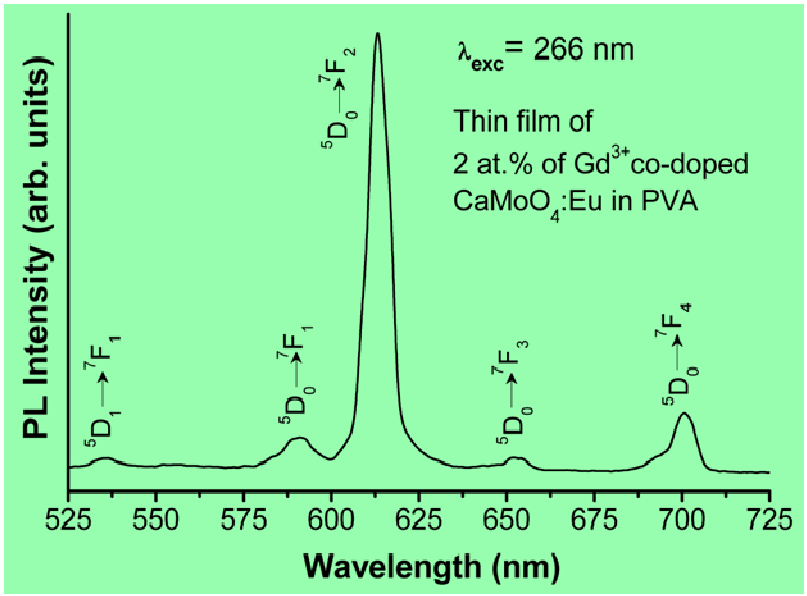

Figure 4.20: Luminescence spectra of PVA thin film of as-prepared 2 at.% Gd^{3+} co-doped $CaMoO_4$:Eu nanoparticles after incorporation of re-dispersed particles at 266 nm excitation.

4.2.3.2.4 Quantum yield study

Luminescence quantum yield (η) of samples is calculated on basis of absolute method. This is related to the number of photons absorbed (α) to number of photons emitted by the sample (ε) as

$$\eta = \frac{\varepsilon}{\alpha} = \frac{\int I_{emission}}{\int I_{solvent} - \int I_{sample}} \tag{4.9}$$

where $I_{emission}$ is luminescence emission spectrum of sample, $I_{solvent}$ is the spectrum of light used to excite only solvent, and I_{sample} is the spectrum of light used for exciting sample in solvent. Detail experiment set up was reported [Singh et al.(2009)]. All spectra are collected using the integrating sphere. Here, solvent is 1 g of PEG dispersed in 100 ml of distilled water. Excitation and emission wavelengths are monitored at 277 nm (absorption peak of Gd^{3+}) and 615 nm. Typical PL spectra of 2 at.% Gd^{3+} co-doped $CaMoO_4$:Eu for the quantum yield are shown in Figure 4.21. The luminescence quantum yields for 2 and 10 at.% Gd^{3+} co-doped $CaMoO_4$:Eu (ASP) are 21 and 80%, respectively. The high quantum efficiency (200%) was reported in Ln^{3+} doped $LiGdF_4$ under VUV excitation [Wegh et al.(1999)].

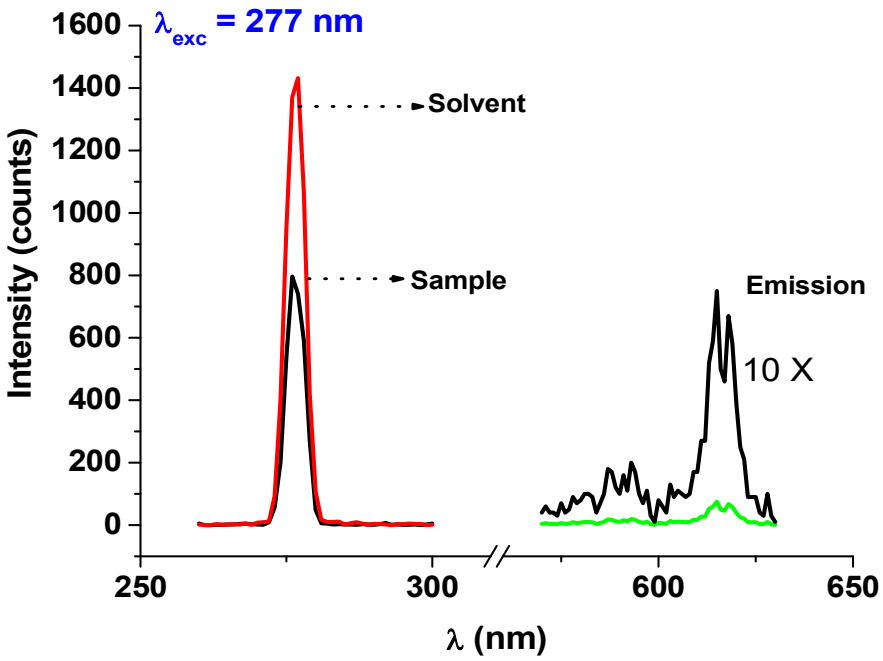

Figure 4.21: PL spectra of 2 at.% Gd^{3+} co-doped $CaMoO_4$:Eu for the quantum yield study.

4.2.3.2.5 Photoluminescence decay study

Photoluminescence decay profile of $^5D_0$ (613 nm) level of Eu^{3+} for ASP, 600 and 900 ^oC annealed samples of Gd^{3+} (0, 5 and 10 at.%) co-doped $CaMoO_4$:Eu samples under 277 and 395 nm excitations have been shown in Figures 4.22-24. Emission wavelength has been fixed at 613 nm. It shows the decay profile of $^5D_0 \rightarrow {}^7F_2$ transition excited at two different excitations ~277 nm (Gd^{3+}/MoO_4^{2-}) and 395 nm (direct excitation of Eu^{3+}).

Typical plot for 600 ^oC annealed 5 at.% Gd^{3+} co-doped $CaMoO_4$:Eu under 277 nm excitation using mono-exponential equation given in equation (3.2) is shown in Figure 25 (a) and the ln(*I*) *vs t* plot is shown in inset figure for the same. Fitting parameters are given in figure itself. From inset of figure (a), it is evident that decay curve deviates from mono-exponential curve fit.

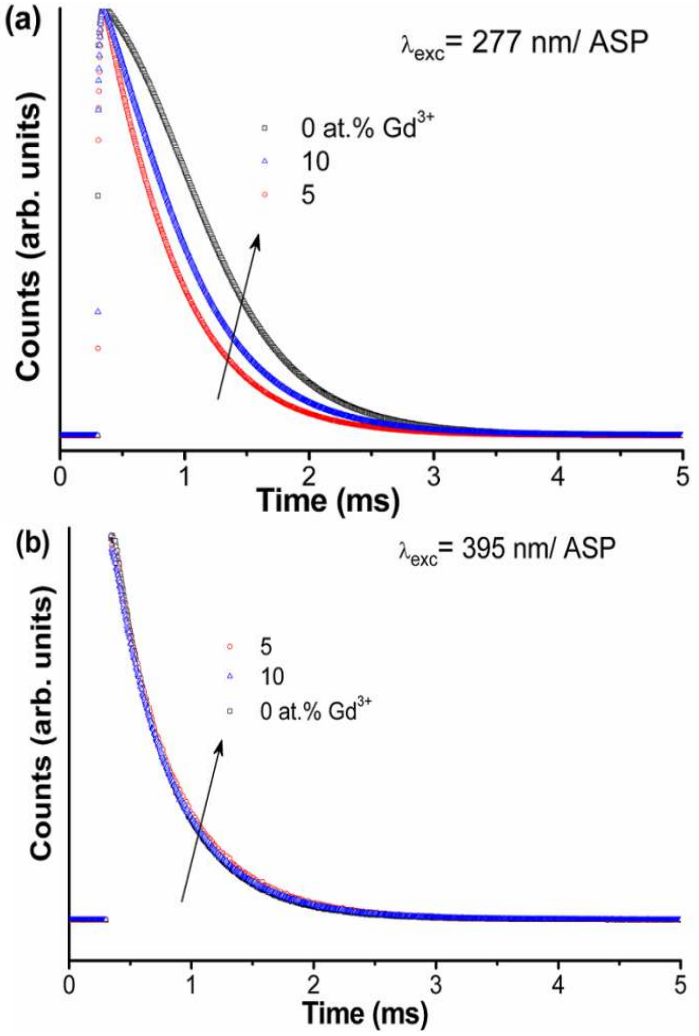

Figure 4.22: Lifetime decay spectra of ASP Gd^{3+} (0, 5 and 10 at.%) co-doped $CaMoO_4$: Eu nanoparticles at (a) 277 and (b) 395 nm excitations.

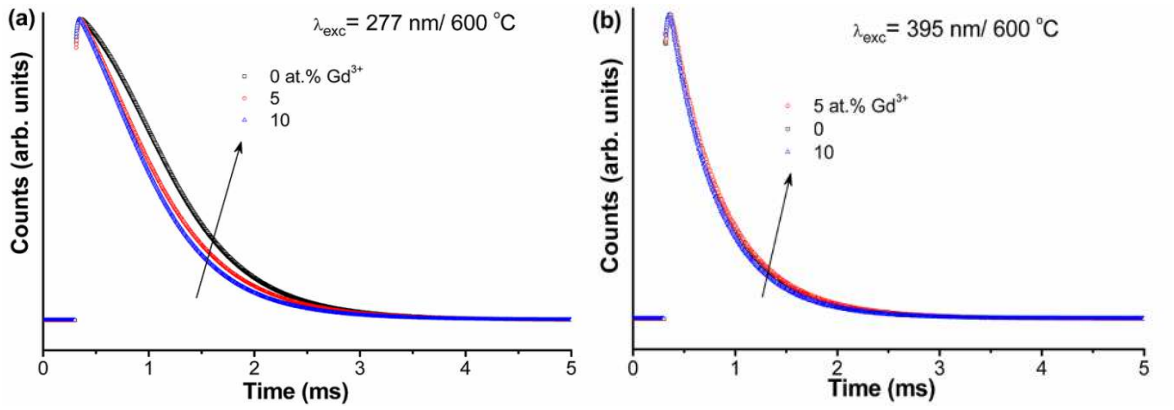

Figure 4.23: Lifetime decay spectra of 600 °C Gd^{3+}(0, 5 and 10 at.%) co-doped $CaMoO_4$:Eu nanoparticles at (a) 277 and (b) 395 nm excitations.

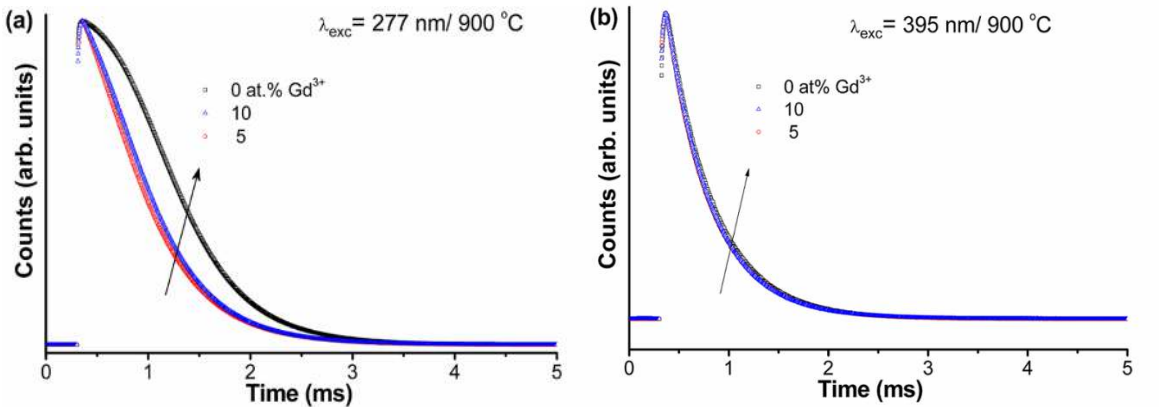

Figure 4.24: Lifetime decay spectra of 900 °C Gd^{3+}(0, 5 and 10at.%) co-doped $CaMoO_4$:Eu^{3+} nanoparticles at (a) 277 and (b) 395 nm excitations.

Therefore, in case of 277 nm (Gd/Mo-O) excitation, luminescence decay curve for $^5D_0 \rightarrow {}^7F_2$ has been fitted using diffusion equation as

$$I = I_1 \exp\left(-t/\tau_1 - Dt^{0.5}\right) - I_2 \exp\left(-t/\tau_2\right) + I_b \qquad (4.10)$$

where I_1, I_2 and I_b are the intensity parameters while D is the diffusion parameter and energy transfer rate. The χ^2 is the goodness of fit and can be expressed as

$$\chi^2 = \frac{\sum_k w_k{}^2 [X_k - F_k]^2}{n} \qquad (4.11)$$

where w_k is a weighting factor for data points ($w_k = \frac{1}{\sqrt{F_k}}$), X_k is the fitted data and F_k is luminescence decay data. Typical fitting of 5 at.% Gd^{3+} co-doped $CaMoO_4$:Eu annealed at 600 °C at 277 nm excitation has been shown in Figure 4.25 (b).

Parameters obtained using equation (5) has been given in figure itself. Fitting parameters obtained for ASP, 600 and 900 ^oC annealed Gd^{3+} co-doped $CaMoO_4$:Eu samples are listed in Table 4.3

Table 4.3: Parameters obtained after fitting [$I = I_1 \exp(-t/\tau_1 - Dt^{0.5}) - I_2 \exp(-t/\tau_2) + I_b$] equation to the decay data of as-prepared, 600 and 900 ^oC samples at 277 nm excitation.

Sample	Gd^{3+} (at.%)	I_1%	τ_1(ms)	D ($S^{-0.5}$)	I_2%	τ_2(ms)	I_b	χ^2
ASP	0	42	0.30	-0.7088	58	0.48	0.0018	0.99997
	5	51	0.46	-1.3651	49	0.58	0.0032	0.99994
	10	53	0.42	-1.3393	47	0.52	0.0017	0.99997
600 ^oC	0	28	0.22	-2.4819	72	0.55	0.0024	0.99998
	5	67	0.43	-0.8641	33	0.48	0.001	0.99998
	10	44	0.37	-2.0001	56	0.58	0.0021	0.99990
900 ^oC	0	39	0.27	-1.3387	61	0.43	0.0009	0.99991
	5	48	0.38	-1.6068	52	0.52	0.0019	0.99995
	10	50	0.42	-1.5977	50	0.56	0.0025	0.99993

There are two components of lifetime. The lifetime (τ_1) associated with Diffusion and energy transfer rate (termed as D) is shorter than another one (τ_2). It means that at initial stage, decay is fast. However τ_1 and τ_2 have almost equal amounts. The τ_2 in case of Gd doped sample is slightly longer than that without Gd. The τ_1 = 0.22-0.46 ms and τ_2 = 0.42-0.58 ms are found.

All decay curves are fitted under 395 nm excitation using bi-exponential curve fitting which is expressed as

$$I = I_1 e\left(\frac{-t}{\tau_1}\right) + I_2 e\left(\frac{-t}{\tau_2}\right) \tag{4.12}$$

where I_1 and I_2 be the intensities at different time intervals and τ_1 and τ_2 be their corresponding lifetimes, respectively. The average lifetime τ_{av} is calculated as

$$\tau_{av} = \frac{I_1\tau_1 + I_2\tau_2}{\tau_1 + \tau_2} \tag{4.13}$$

Bi-exponential fitting behaviour corresponds to inhomogeneous distribution of activator ions (Eu^{3+}) in $CaMoO_4$ host matrix. The shorter lifetime (τ_1) has more contribution than longer one (τ_2). The amount of longer lifetime (τ_2) decreases upon increasing annealing. Even, 900 ^oC annealed samples follow mono-exponential decay. Average lifetime (τ_{av}) of sample doped with Gd has longer lifetime than that without Gd. The τ_1 = 0.41-0.50 ms and τ_2 = 0.65-1.29 ms are found. Fitting parameters ((I_1, τ_1, I_2, τ_2, τ_{av} and χ^2) calculated using bi-exponential curve fit for ASP, 600 and 900 ^oC annealed samples of Gd^{3+} co-doped $CaMoO_4$:Eu samples are listed in Table 4.4.

Table 4.4: Parameters obtained after bi-exponential fit to the decay data of as-prepared, 600 and 900 ^oC samples at 395 nm excitations

Sample	Gd^{3+} (at.%)	I_1	τ_1 (ms)	I_2	τ_2 (ms)	τ_{av} [a]/(ms)	χ^{2b}
ASP	0	1.8211	0.4179	0.4304	0.6567	0.4826	0.99993
	5	1.9557	0.4944	0.0356	1.3664	0.5362	0.99981
	10	1.9856	0.4835	0.0311	1.2477	0.5132	0.99989
600 ^oC	0	2.0226	0.4796	0.0933	0.9576	0.5199	0.99992
	5	2.0045	0.5021	0.0778	1.0049	0.5383	0.99995
	10	2.1341	0.4776	0.0178	1.2905	0.4955	0.99995
900 ^oC	0	2.2791	0.46667	-	-	0.46667	0.99996
	5	2.2577	0.4368	0.0622	0.8959	0.4614	0.99993
	10	2.1826	0.4429	0.1375	0.5772	0.4531	0.99997

[a] $\tau_{av} = \frac{I_1\tau_1 + I_2\tau_2}{\tau_1 + \tau_2}$. [b] $\chi^2 = \sum_k \frac{w_k^2[X_k - F_k]^2}{n}$ is goodness of fit, w_k is weighting factor for data points) and X_k and F_k be the calculated and measured life time data

Typical bi-exponential fitting of 5 at.% Gd^{3+} co-doped $CaMoO_4$:Eu annealed at 600 ^oC under 395 nm excitation is shown in Figure 4.25 (c) and Average life time value was reported as ~0.459 ms for 5 at.% Eu^{3+} doped $CaMoO_4$ under 398 nm excitation.[Parchur, et al.(2011a)]

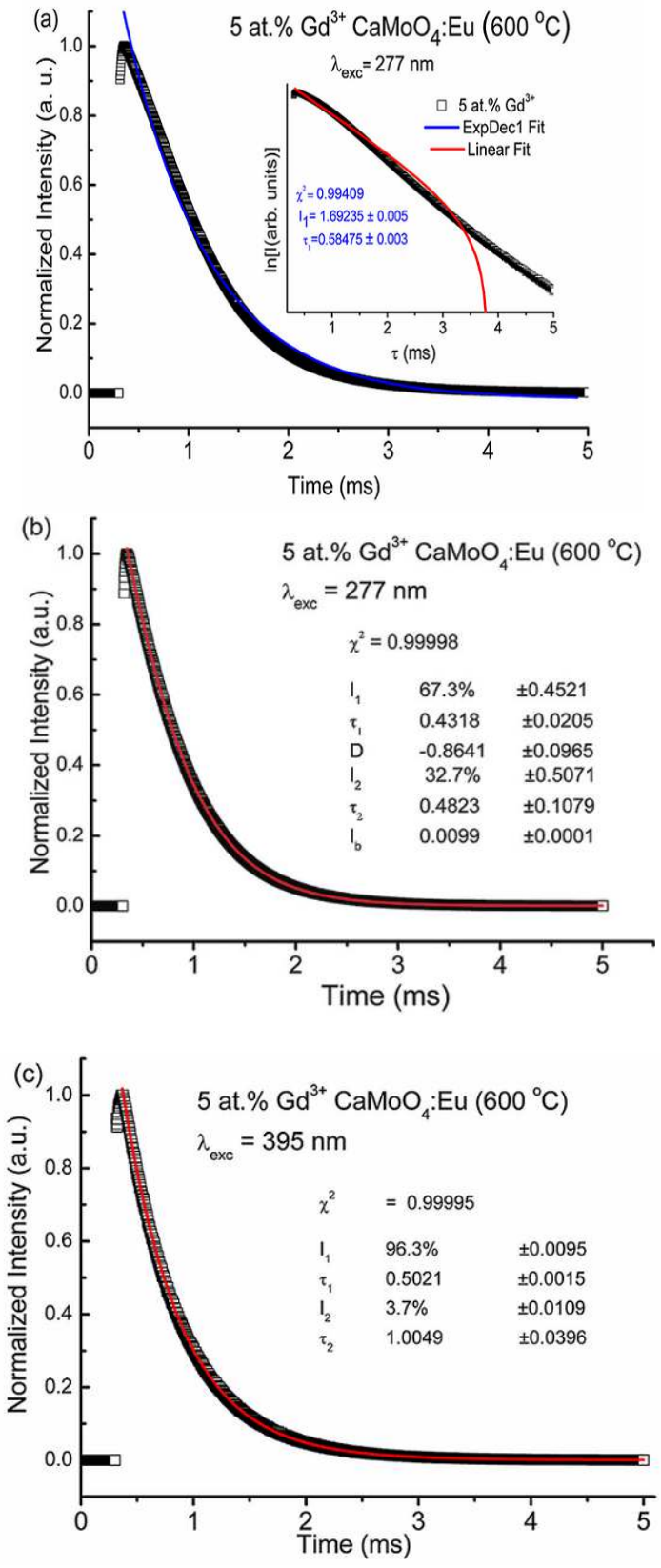

Figure 4.25: (a) Mono- (b) diffusion equation fittings to luminescence decay curve (613 nm) of 600 °C annealed 5 at.% Gd^{3+} co-doped $CaMoO_4$:Eu (λ_{exc}=277 nm). Fitting parameters are shown in figures itself. Inset of (a) shows the ln(*I*) *vs t* plot. and (c) bi-exponenetail fitting to the decay curve of 5 at.% Gd^{3+} co-doped $CaMoO_4$:Eu (λ_{exc}=395 nm).

Typical bi-exponential decay fitting for 10 at.% Gd^{3+} co-doped $CaMoO_4$:Eu samples annealed at 900 °C and their weighted residuals is shown in the Figure 4.26. The residuals decay plot is more informative and in fact it demonstrates that where the misfit occurs in the curve.

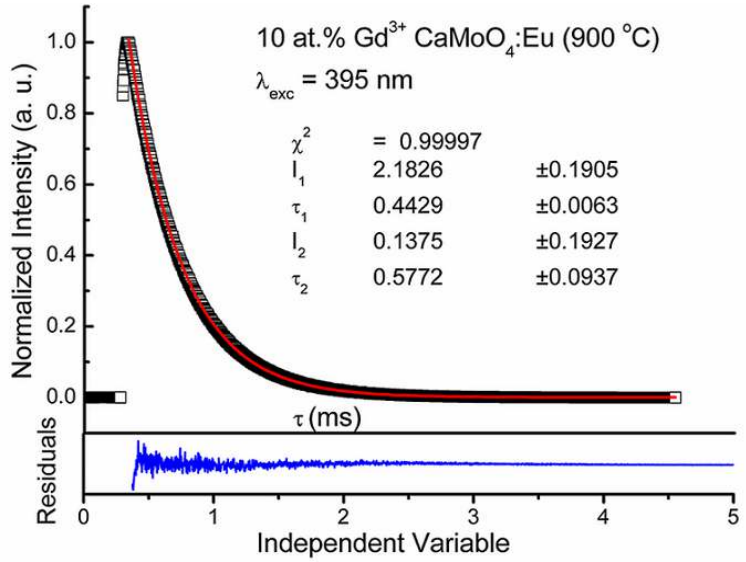

Figure 4.26: Typical Bi-exponential fittings with residuals to the luminescence decay curve (613 nm) of 10 at.% Gd^{3+} co-doped $CaMoO_4$:Eu annealed at 900 °C (λ_{exc}= 395 nm). Bottom portion of figure show the residual vs. Independent Variable.

In case of 0 at.% Gd^{3+} co-doped $CaMoO_4$:Eu sample annealed at 900 °C under 395 nm excitation, we observed that the decay curve show deviation from its bi-exponential (shown in Figure 4.27(a)) curve fit and fitted well with mono-exponential function (Shown in Figure 4.27(b))).

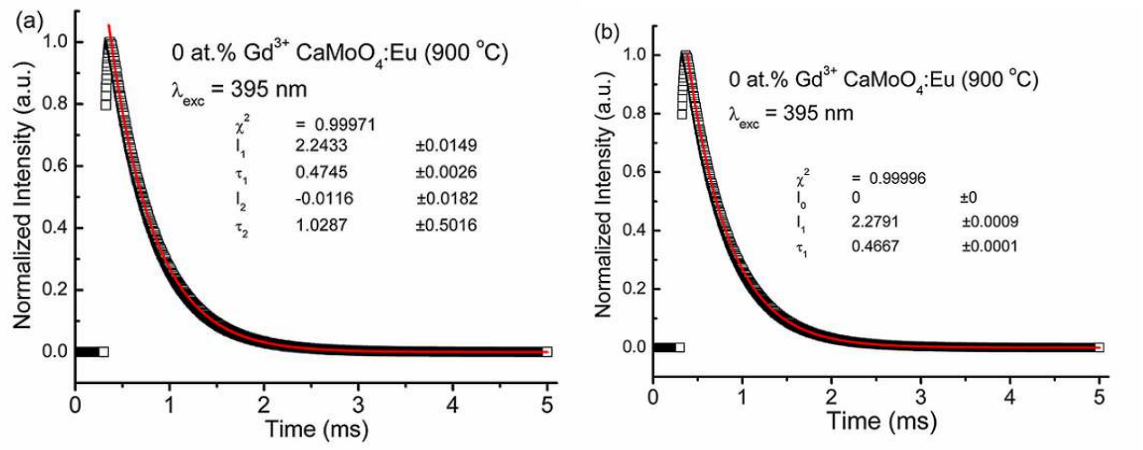

Figure 4.27: (a) Bi- (b) mono-exponential curve fits to luminescence decay curve (613 nm) of 0 at. % Gd^{3+} co-doped $CaMoO_4$:Eu annealed at 900 °C (λ_{exc}= 395 nm).

Calculated lifetime values under 395 nm excitation of 0, 5 and 10 at.% Gd^{3+} co-doped $CaMoO_4$:Eu for ASP, 600 and 900 ^oC using mono-exponential curve fit were listed in Table 4.5.

Table 4.5: Parameters obtained after mono-exponential fit to the decay data of as-prepared, 600 and 900 ^oC samples at 395 nm excitations.

Sample	Gd^{3+} (at.%)	I_1	τ_1 (ms)	χ^2
ASP	0	2.1416	0.4766	0.99979
	5	1.9459	0.5139	0.99969
	10	1.9807	0.4985	0.99982
600 ^oC	0	2.0645	0.5064	0.99983
	5	2.0363	0.5261	0.99987
	10	2.1239	0.4867	0.99991
900 ^oC	0	2.2791	0.46667	0.99996
	5	2.2793	0.4526	0.99988
	10	2.2999	0.4531	0.99996

The average life time values for 5 and 10 at.% Gd^{3+} doped 900 ^oC annealed samples show decrement as compared to ASP and 600 ^oC annealed samples. Wang and his co-workers(2007) reported the decrease in lifetime values for Bi^{3+} co-doped $CaMoO_4$:Eu nanophosphors. Similar type of results are observed in cases of $Ca_2(Gd_{1-x}A_x)_8Si_6O_{26}$, A= Eu, Tb nano phosphor on annealing the samples above 800 ^oC [Raju, et al.(2010)]. It is worthwhile to mention the lifetime values reported in literature for some other Eu^{3+} doped hosts. Since such comparison will gives an idea about the effect of Gd^{3+} doping and surface defects associated with the samples. Some of the reported life time of Eu^{3+} doped other hosts materials: Y_2O_3:Eu, Gd_2O_3:Eu, YVO_4:Eu, $GdVO_4$:Eu, and $LaPO_4$:Eu are ~1.763, 1.56, 0.247, 0.583 and 3.56 ms, respectively [Jia, et al.(2009), Liu, et al.(2010), Luwang, et al.(2011), Phaomei, et al.(2010)].

Radiative rate constant is calculated from reciprocal of lifetime ($K = 1/\tau_{av}$). Values of radiative rate constants using bi-exponential curve fit under 395 nm excitation for 0, 5 and 10 at.% Gd^{3+} co-doped $CaMoO_4$:Eu are $2.17x10^3$, $1.96x10^3$ and $2.04x10^3$ s^{-1}, respectively for ASP samples; $2.0x10^3$, $1.92x10^3$ and $2.08x10^3$ s^{-1}, respectively for 600 ^oC annealed samples; and $2.12x10^3$, $2.27x10^3$ and $2.27x10^3$ s^{-1}, respectively for 900 ^oC annealed sample. Radiative rate constants for mono-exponential curve fit for 0, 5 and 10 at.% Gd^{3+}co-doped $CaMoO_4$:Eu under 395 nm excitation for ASP, 600 and 900 ^oC annealed samples are given in Table 4.6.

Table 4.6: Radiative rate constants of Gd^{3+} co-doped $CaMoO_4$:Eu samples after mono-exponential curve fit to the luminescence decay curve under 395 excitation.

Sample	Gd^{3+} (at.%)	Radiative rate constant (ms^{-1})
ASP	0	2.0982
	5	1.9459
	10	2.0061
600 ^oC	0	1.9747
	5	1.9008
	10	2.0547
900 ^oC	0	2.1428
	5	2.2095
	10	2.2071

4.2.3.2.6 CIE study

The Commission Internationale de l'Eclairage (CIE) study have been performed on Gd^{3+} (0, 2, 5, 7 and 10 at.%) co-doped $CaMoO_4$:Eu samples for ASP, 600 and 900 ^oC annealed samples. Typical CIE co-ordinates of 5 at.% Gd^{3+} co-doped $CaMoO_4$:Eu for ASP, 600 and 900 ^oC are found to be (0.5334, 0.3711), (0.5331, 0.3708) and (0.6068, 0.3614), respectively. Detailed analysis of CIE co-ordinates of Gd^{3+}(0, 2, 5, 7 and 10 at.%) co-doped $CaMoO_4$:Eu samples for ASP, 600 and 900 ^oC annealed have been given in the Table 4.7.

Table 4.7: Variation of CIE co-ordinates of ASP, 600 and 900 ^oC annealed Gd^{3+} (0, 2, 5, 7 and 10 at.%) co-doped $CaMoO_4$:Eu samples.

	CIE chromaticity co-ordinates					
	ASP		**600 ^oC**		**900 ^oC**	
Gd^{3+} (at.%)	**x**	**y**	**x**	**y**	**x**	**y**
0	0.4731	0.3685	0.4726	0.3679	0.6127	0.3714
2	0.5171	0.3704	0.5171	0.3703	0.6205	0.3681
5	0.5334	0.3711	0.5331	0.3708	0.6068	0.3614
7	0.5785	0.3713	0.5785	0.3713	0.5979	0.3652
10	0.5879	0.3659	0.5879	0.3659	0.5937	0.3663

4.2.4 Conclusions

From PLE study, strong overlapping of Eu-O and Gd^{3+}/Mo-O charge transfer bands is observed. Absorption/excitation intensity increases with Gd^{3+} indicating energy transfer from Gd^{3+}/Mo-O to Eu^{3+}. Band gap decreases with annealing. In the photoluminescence study of Gd^{3+} co-doped $CaMoO_4$:Eu, the optimum PL intensity values are found at 2, 7 and 10 at.% for ASP, 600 and 900 ^oC samples, respectively. Enhancement of luminescence is found with annealing due to extent of decrease of non-radiative rates arising from surface dangling bonds and –OH ions to surface of the samples. The asymmetric ratios (A_{21}) of electric to magnetic dipole transitions are found to be in the range of ~12-16, which is relative higher than those of reported ones. The room temperature emission spectrum is dominated by the $^5D_0 \rightarrow {}^7F_2$ transition at 613 nm. Emission quantum yields up to 80% was obtained under excitation at 277 nm for ASP 10 at.% Gd^{3+} co-doped $CaMoO_4$:Eu. From the photoluminescence decay studies on direct excitation at 395 nm and indirect excitation at 277 nm, energy transfer from Gd/Mo-O CT band to Eu^{3+} occurs. PL intensity variations have been studied in polar solvents; and found that these nanoparticles are dispersible and these dispersed particles can be incorporated in polyvinyl alcohol to make a film. Film shows the dark red emission after UV-radiation which can be useful in display devices. The CIE co-ordinates for 5 at.% Gd^{3+} co-doped with $CaMoO_4$:Eu^{3+} for ASP, 600 and 900 ^oC are found to be (0.5334, 0.3711), (0.5331, 0.3708) and (0.6068,0.3614), respectively. Through this study, we have demonstrated the high quality luminescent material by incorporating Gd^{3+} ion, which is of great importance in improving luminescence efficiency of the red phosphor at a much lower cost.

★★★★★★